

Ionization Structure and Spectra of Iron in Gaseous Nebulae

Manuel A. Bautista & Anil K. Pradhan

Department of Astronomy, The Ohio State University

174 West 18th Avenue, Columbus, OH 43210-1106

Received _____; accepted _____

arXiv:astro-ph/9710073v1 7 Oct 1997

ABSTRACT

The emission spectra and the ionization structure of the low ionization stages of iron, Fe I–IV, in gaseous nebulae are studied. This work includes: (i) new atomic data: photoionization cross sections, total e-ion recombination rates, excitation collision strengths, and transition probabilities calculated under the Iron Project by the Ohio State atomic-astrophysics group; (ii) detailed study of excitation mechanisms for the [Fe II], [Fe III], and [Fe IV] emission, and spectroscopic analysis of the observed IR, optical, and UV spectra; (iii) study of the physical structure and kinematics of the nebulae and their ionization fronts. Spectral analysis of the well observed Orion nebula is carried out as a test case, using extensive collisional-radiative and photoionization models. It is shown that the [Fe II] emission from the Orion nebula is predominantly excited via electron collisions in high density partially ionized zones; radiative fluorescence is relatively less effective. Further evidence for high density zones is derived from the [O I] and [Ni II] spectral lines, as well as from the kinematic measurements of ionic species in the nebula. The ionization structure of iron in Orion is modeled using the newly calculated atomic data, showing some significant differences from previous models. The new model suggests a fully ionized H II region at densities on the order of 10^3 cm^{-3} , and a dynamic partially ionized H II/H I region at densities of $10^5 - 10^7 \text{ cm}^{-3}$. Photoionization models also indicate that the optical [O I] and [Fe II] emission originates in high density partially ionized regions within ionization fronts, thereby confirming the general Fe II/O I correlation in H II regions determined in earlier studies. The gas phase iron abundance in Orion is estimated from observed spectra, including recently observed [Fe IV] lines.

Subject headings: H II regions – ISM:individual (Orion Nebula) –
ISM:abundances – ISM:structure – atomic processes – star:formation

1. Introduction

The spectra, ionization structure, and the abundance of iron are valuable indicators of the physical conditions and the chemical evolution of astrophysical objects. First, owing to its relatively high abundance and the complex atomic structure of Fe ions, a large number of spectral lines are observed across most of the electromagnetic spectrum. Secondly, several ionization stages of iron may be observed from different zones within the same object. The low ionization stages of iron, Fe I–IV, generally span the physical and the ionization structure of gaseous nebulae, from the cool neutral regions and partially ionized zones, to the fully ionized regions close to the ionizing source. For instance, since the ionization potentials of Fe I and Fe II are 7.6 and 16.2 eV respectively, compared with 13.6 eV for H I, the Fe II spectrum commonly traces the conditions in partially ionized regions and ionization fronts where Fe II is shielded by H I. Beyond 54.4 eV, the ionization potential of Fe IV, the photon density from the radiation field of O and B stars is too low to effect higher ionization of iron (Osterbrock 1989). Thus, a combined study of Fe I–IV should provide detailed information on the structure and physical conditions of the HII region. Thirdly, while iron is primarily formed in the interstellar medium (ISM) by supernovae, it is a refractory element and its gas phase abundance constrains both the chemical enrichment of the ISM and the formation of dust grains.

As the best observed diffuse H II region, the Orion nebula is commonly used as a “benchmark” for nebular studies. The present study aims at an understanding of some aspects of low-excitation photoionized nebulae through the analysis of the ionization structure and spectra of Fe I–IV in Orion based on: (i) new calculations of atomic data for Fe I–IV, necessary for ionization equilibrium and spectral formation modeling, (ii) study of ionization balance, excitation mechanisms, and radiative transfer of the spectra of Fe ions; (iii) study of the physical structure of nebulae including density and temperature variations

and kinematic effects.

Despite the importance of low ionization stages of iron in laboratory and astrophysical plasmas, accurate atomic data for these ions were not available until the recent advances by the Iron Project (hereafter IP; Hummer et al. 1993). The IP calculations are carried using the close coupling approximation and the R-matrix method that is presently the most accurate method for calculating photoionization, recombination, and excitation cross sections. The calculations are rather involved, and computationally intensive, owing to the complex electron-electron correlation effects, the large number of coupled atomic states of iron ions, and the complex resonance structures present in the cross sections. A brief discussion of these calculations and the atomic data is presented in Section 2.

Excitation mechanisms for iron spectra are of particular interest. The forbidden [Fe II] emission is known to be exceptionally strong in most gaseous nebulae, such as Orion (e.g. Grandi 1975; Osterbrock et al. 1992), supernova remnants (e.g. Dennefeld & Péquignot 1983; Dennefeld 1986; Henry et al. 1984; Hudgins et al. 1990; Rudy et al. 1994), Seyfert galaxies (e.g. Osterbrock et al. 1990), and circumstellar nebulae of luminous blue variables (e.g. Stahl & Wolf 1986; Johnson et al. 1992). Bautista, Pradhan, & Osterbrock (1994) found that the optical [Fe II] emission in Orion seems to be excited in regions with high electron densities of $\sim 10^5 - 10^7 \text{ cm}^{-3}$. Further, (Bautista & Pradhan 1995a; BP95a hereafter) presented evidence that [Fe II] emission in Orion stems from partially ionized zones (PIZs), where hydrogen and oxygen are mostly neutral, and collisionally excited [O I] lines are observed. At about the same time, in order to explain the anomalously intense [Ni II] optical emission from a variety of astrophysical objects, Lucy (1995) showed that the [Ni II] emission in Orion and the circumstellar nebula P Cygni could be excited by fluorescence via the background UV continuum, and suggested that [Fe II] optical emission may be similarly affected by UV fluorescence. This photo-excitation mechanism for [Ni II]

and [Fe II] was further examined by Bautista, Peng, & Pradhan (1996; BPP hereafter). It was concluded that owing to the differences in the atomic structure, fluorescence excitation is less effective for [Fe II] than for [Ni II] and appeared relatively unimportant for Orion. In contrast, Baldwin et al. (1996; B96 hereafter) modeled the optical [Fe II] emission from Orion and found UV fluorescence to be a viable mechanism as opposed to the high electron densities deduced by BPP. They argued that the UV lines of Fe II that dominate the photoexcitation are optically thick and by including self-shielding, a process not considered in BPP, the observed [Fe II] spectra could be reproduced at electron densities of $\sim 10^4$ cm^{-3} . The collisional and fluorescent excitation, including optical depth effects, are further investigated herein (Section 3.1). Our results, and those reported by B96, are compared with several independent spectroscopic measurements of Orion.

In Sections 3.2 and 3.3 we investigate the excitation of [Fe III] and [Fe IV] lines to study the physical conditions in the emitting region and the abundance of iron in Orion. It is expected that optical [OI] emission arises from the same partially ionized regions as the [FeII] spectrum. In Section 4 we discuss the [OI] line diagnostics with presently available measurements.

The role of kinematics in the structure and physical properties of photoionized nebulae is also investigated. In diffuse H II regions, such as Orion and M17, the ionizing radiation from hot stars drives dissociation (D) and ionization (I) fronts into a dense molecular cloud on the far side of the nebula. The newly ionized gas is driven by a strong pressure gradient, the “champagne” effect (e.g. Bodenheimer et al. 1979), and results in a stratification of velocities and ionization states of the emitting ions in the H II regions. Such a correlation between velocities and ionization was first observed by Kaler (1967) and is discussed in Section 5 of the present paper. In Section 6, some discrepancies between the predictions of current static photoionization models and the observed structure of nebulae are pointed out.

Photoionization models of Orion, taking into account the high density ionization, fronts are presented together with the predicted spectra of neutral and low ionization species, e.g. O I and Fe II.

Finally, we derive gas phase Fe/O abundance ratios in different emitting regions in Orion from spectroscopic data (Section 7). Section 8 summarizes the results and the conclusions.

2. Atomic Data

We present a review of the atomic data for spectroscopic analysis and radiative modeling of Fe I–IV. This includes: electron-impact excitation rate coefficients (Υ 's), radiative transition probabilities (A -values), photoionization cross sections, and recombination rate coefficients. These data have been calculated at Ohio State in collaboration with S. N. Nahar and H. L. Zhang. Table 1 summarizes the extent of the computed data employed in the present work. The new IP data complements or supersedes the radiative data for the iron ions obtained under the Opacity Project (Seaton et al. 1994).

With the exception of experimentally measured energy levels (compiled by Sugar and Corliss 1985) and oscillator strengths for dipole allowed and intercombination transitions in FeII, all other atomic data for iron ions are computed theoretically. The complexity of the atomic structure of these ions places formidable demands on large-scale computations using the most accurate methods, and the accuracy of some of the data may be constrained by present computational resources. Nevertheless, by comparing several sets of independent calculations for a given ion, and for different but related atomic processes such as bound-bound and bound-free radiative transitions, it is possible to derive some conclusions about the uncertainties of the data and the reliability of the resulting atomic models.

2.1. Collision strengths and transition probabilities

The collisional-radiative models used in the present study employ the Maxwellian averaged effective collision strengths and transition probabilities for forbidden transitions obtained as described below.

2.1.1. *Fe II*

Recently, collisional data for electron impact excitation of Fe II were provided by the close-coupling calculations of Pradhan & Zhang (1993) and Zhang & Pradhan (1995a; ZP95 hereafter). Collision strengths and rate coefficients were given for 10,011 transitions among 142 fine structure levels of 38 LS terms dominated by the configurations $3d^6 4s$, $3d^7$, and $3d^6 4p$. However, these data sets did not include levels with multiplicity $(2S + 1) = 2$ or levels dominated by the $3d^5 4s^2$ (e.g. the $a^6 S_{5/2}$ level). In order to complement ZP95 and to check on the accuracy of these data for optical transitions, we carried out a new calculation (Bautista & Pradhan 1996; hereafter, BP96) including the lowest 18 multiplets of Fe II with 52 fine structure levels and 1326 transitions, using an improved wavefunction representation of the ion. Although the BP96 collision strengths exhibit background values in very good agreement with those of ZP95, there are differences between the two sets owing to the resonance structures belonging to the odd parity terms of the $3d^6 4p$ configuration. In order to estimate the effect of the coupling to the odd parity terms, we have carried out a new 23 state close coupling calculation (23CC) that includes the $3d^6 4p \ z^6 D^o, z^6 F^o, z^6 P^o, z^4 F^o$, and $z^4 D^o$ terms in addition to the 18 multiplets in BP96. Some additional resonance structures, absent in BP96, enhance the Maxwellian averaged collision strengths $\Upsilon(T)$, resulting in better agreement with ZP95 for the transitions common to the two datasets. Table 2 presents a comparison between the Υ -values at 10^4K from the new 23CC calculation and the BP96 and ZP95 calculations for transitions from the ground state $^6 D_{9/2}$ with

$\Upsilon > 0.1$. Only a few such transitions show a significant difference with respect to BP96, e.g. the ${}^6D_{9/2} - {}^6S_{5/2}$ transition for which $\Upsilon(10^4\text{K})$ increased from 0.399 to 0.857 due to additional resonance contributions. The present 23CC results are well correlated with those of ZP95, particularly for transitions from the levels of the ground ($a\ {}^6D$) and first excited ($a\ {}^4F$) multiplets which dominate the collisional excitation of the ion. There are, however, two sets of transitions, $a\ {}^6D_i - a\ {}^4F_j$ and $a\ {}^4F_i - b\ {}^4F_j$, for which the collision strengths differ by factors of two to three. This discrepancy suggests that there may be some difficulties in representing the states of FeII with a $3d^7$ configuration, which would require a more extensive target basis set than used so far. Nevertheless, the uncertainty in excitation rates for these $3d^7$ levels has only a small effect on the near-IR and optical line ratios, as shown in Sections 3.1 and 3.2. For the present work we construct a 159 level system for Fe II that uses data for the 142 levels in ZP95, and the new results from the 23CC calculation.

Accurate transition probabilities for forbidden transitions are difficult to calculate because very accurate wavefunctions are needed to obtain the weak relativistic electric quadrupole and magnetic dipole probabilities with very small Einstein A-coefficients. For Fe II such computations are especially challenging owing to the number of algebraic terms involved. The first A-values for the [Fe II] IR and optical lines were reported by Garstang (1962). Nussbaumer & Storey (1988) provided a more accurate set of A-values for IR and near-IR transitions that result from the 16 fine structure levels of the first 4 LS terms, $3d^64s\ a^6D$, a^4P and $3d^7\ a^4F$, a^4D , using the program SUPERSTRUCTURE (Eissner et al. 1974). Recently, Quinet et al. (1997) have reported more extensive calculations for the [Fe II] transitions, using SUPERSTRUCTURE and the semi-empirical code by Cowan (1981). The differences between these data and those of Nussbaumer & Storey and Garstang’s are small, a few percent for most transitions, but they reach up to a factor of two for some transitions. Computational limitations restricted Quinet et al. from explicitly including some important configurations that were included earlier by Nussbaumer and

Storey (1988), such as $3d^54d^2$ and $3d^54f^2$, in the configuration interaction expansion. The effect of excluding these configurations was estimated to be approximately 25-30% for many transitions.

Some indication of the accuracy of the different A-values data sets may be obtained by comparing with observations for pairs of lines that originate from the same upper level; then the intensity ratio depends only on the known energy differences and the A-values. In Tables 3 and 4 we compare such line ratios, for IR and optical lines respectively, with observations of the Herbig-Haro object, HH1. This object exhibits particularly strong [Fe II] emission while emission from HI and HeI are inhibited. Similar comparisons have been carried out using spectra of various nebulae and supernova remnants. Table 3 reveals very good agreement, within $\sim 5\%$ for most line ratios, between the data by Nussbaumer & Storey and the observations, but the data by Quinet et al. yield significant discrepancies. One particularly interesting ratio is $I(1.257\mu\text{m})/I(1.644\mu\text{m})$, comprising the strongest [Fe II] lines in the near-IR region. This ratio is useful, for example, in the diagnosis of dust extinction (e.g. Dennefeld 1982, 1986; Bautista, Pogge, & Depoy 1995). The observed ratio of 1.34 agrees within 2% with the expected value from the Nussbaumer & Storey data, while the Quinet et al. data yield a ratio nearly 30% lower. The line ratio comparison for optical lines in Table 4 shows some differences between observations and Garstang's data, $\sim 30\%$. The differences with respect to the data by Quinet et al. are somewhat larger.

Based on these comparisons we adopt the data by Nussbaumer & Storey for the IR transitions, and Garstang's data for the rest. We estimate that these data sets may be uncertain to the 5-10% and 30-40% levels respectively. More calculations of transition probabilities for the optical [Fe II] lines are needed.

2.1.2. *Fe III*

Recently, Zhang & Pradhan (1995b) and Zhang (1996) reported an extensive set of collision strengths for transitions among 83 LS terms and 219 fine structure levels. They investigated and found the relativistic effects on the collision strengths for the low-lying forbidden transitions to be small, but the effects of resonances and channel couplings to be considerable. They also reported good agreement between a much smaller 7-term calculation and earlier results by Berrington et al. (1991). However, the full 83-term calculation yields resonances that enhance the Υ -values by up to a factor of two. As part of the IP series of publications, Zhang (1996) has provided the complete dataset of the Maxwellian averaged Υ -values for the 23,871 transitions among 219 levels in Fe III (Table 1).

Only two calculations of transition probabilities for [Fe III] lines have been reported. The first calculation was carried out by Garstang (1957). More recently, Nahar & Pradhan (1996) presented new A-values for a larger set of forbidden transitions than the Garstang work, as well as for a large number of dipole allowed transitions. In general, the results of Nahar & Pradhan agree within $\sim 30\%$ with those of Garstang for the transitions common to the two datasets, with some differences of factors of two or higher. The differences are sufficient to significantly affect several diagnostic line ratios; a comparison with available spectroscopic observations (line ratios) shows that the new forbidden A-values of [Fe III] should be preferred (Nahar and Pradhan 1996).

2.1.3. *Fe IV*

The latest collisional calculation for Fe IV has been carried out by Zhang & Pradhan (1997). This work includes transitions among 49 LS terms and 140 corresponding fine

structure levels, dominated by the $3d^5$, $3d^44s$ and $3d^44p$ configurations. Zhang & Pradhan also did a 5-term calculation whose results compare very well, within $\sim 5\%$ or better, with the earlier 4-term ($3d^5 : ^6S, ^4G, ^4P$, and 4D) calculation of Berrington & Pelan (1995; some of these values were revised in an Erratum by Berrington & Pelan 1997). However, Zhang and Pradhan (1997) find that the larger 49-term expansion, including the couplings to the $3d^4 4p$ odd parity terms, leads to resonance structures that enhance the Υ -values by 20 to 50% for many transitions over the Berrington and Pelan data. We expect the overall uncertainties in the Zhang and Pradhan data to be 10-30%.

The only calculation of A-values for [Fe IV] lines that has been reported is that of Garstang (1958). Spectroscopic observations of these lines are very scarce. Therefore, no checks on the reliability of these data can be made. New calculations of forbidden transition probabilities that take into account important spin-orbit and spin-spin relativistic perturbations are needed.

2.2. Photoionization cross sections and recombination rate coefficients

The photoionization models depend on the accuracy and consistency of the photoionization and the recombination data. During the past few years the close coupling approximation has been extended to a unified treatment of electron-ion recombination that includes both radiative and dielectronic recombination processes (Nahar and Pradhan 1992; 1994a). Further, since the same target eigenfunction expansion is employed for the photoionization and the recombination calculations, the photoionization/recombination data are self-consistent. Photoionization cross sections and the unified electron-ion recombination rate coefficients have been computed for all iron ions of interest herein: Fe I–IV.

The new photoionization cross sections differ substantially, by up to orders of magnitude in the important near-threshold regions, from earlier calculations by Reilman and Manson (1979; RM hereafter) and Verner et al. (1993), both using the central field approximation that neglects the spin and angular multiplet atomic structure. Their results contain discontinuous and unphysical jumps in the photoionization cross sections and underestimate the Fe I photoionization cross sections by up to three orders of magnitude (Bautista and Pradhan 1995b, Bautista 1997), the Fe II and Fe III cross section by up to one to two orders of magnitude (Nahar & Pradhan 1994b; Nahar 1996a), and the Fe IV and Fe V cross sections by about one order of magnitude (Bautista & Pradhan 1997; Bautista 1996). The present photoionization cross sections also differ by orders of magnitude from the calculations by Sawey & Berrington (1992) who used a restricted set of eigenfunction expansions for Fe I–IV that did not include sufficient configuration interaction. At high energies, however, the present photoionization cross sections are in reasonable agreement with those obtained from the central field type approximations (expected to be reliable at high energies). It is also of interest to note that the present ground state photoionization cross section of Fe I is in good agreement with that computed by Kelly (1972) using the many-body perturbation method. Fig. 1 shows the ground state photoionization cross sections of Fe I–V together with several previous results. The preponderance of the extensive resonance structures, and their effect on the effective cross sections, is readily discernible.

Unified and total electron-ion recombination coefficients have been recently calculated for Fe I (Nahar, Bautista, & Pradhan 1997), Fe II (Nahar 1997), Fe III (Nahar 1996b), and Fe IV (Nahar, Bautista, & Pradhan; to be submitted). The computations employ the same close coupling expansions and wavefunctions as used in the photoionization calculations. This enables, for the first time, complete consistency between photoionization and recombination data in the photoionization models. The new recombination rates for

Fe I–III are shown in Fig. 2, and compared with previous results by Woods et al. (1981). The new rates for Fe I and Fe II are about a factor of 5 higher than those by Woods et al. in the temperature range 10^3 to 10^4 K. For FeIII the differences are about a factor of 2 at $T = 10^4$ K. An interesting feature of the new unified rates is that at high temperatures, where dielectronic recombination dominates the total recombination (around the large ‘bump’), the present rates are substantially lower than the rates derived from the Burgess General Formula (used by Woods et al.) that is often employed. This large reduction is due to autoionization into the numerous excited states of the target ion, not considered in the Burgess formula.

3. Analysis of the Iron Emission Spectra

Spectral diagnostics of iron ions with several collisional-radiative models and observations in different wavelength regions are described.

3.1. The optical [Fe II] lines

In previous work BPP considered two different collisional-radiative (CR) models for Fe II: a model including the lowest 52 even parity levels (doublets, quartets, and sextets) and a 142 level model including even and odd parity levels with multiplicities $(2S+1) = 4$ and 6. This larger model was used to investigate the fluorescence excitation mechanism. For the present work we have constructed an extended 159-level CR model for Fe II that combines the previous 142 quartet and sextet levels with the lowest doublet levels ($a\ ^2G_j, a\ ^2P_j, a\ ^2H_j, a\ ^2D_j, b\ ^2P_j, b\ ^2H_j, a\ ^2F_j$, and $b\ ^2G_j$) and the previously omitted $4s^2\ ^6S_{5/2}$ level. Dipole allowed and intercombination transition probabilities, necessary for fluorescent excitation, are taken from the compilation of experimental and solar data

by Giridhar & Ferro (1995), when available, and from Nahar (1995) for the rest of the transitions. An energy level diagram for Fe II is shown in Fig. 3. Many of the lines observed in Orion’s optical and near-IR spectra are also marked in this figure.

BPP discussed that, unlike the case of Ni II (Lucy 1995) where all levels participating in fluorescent excitation have the same spin multiplicity (doublets), photoexcitation of Fe II is a relatively inefficient mechanism and the critical densities for fluorescence of most lines are only of the order on 10^4 to 10^5 cm^{-3} for the radiation field in Orion. This is because the ground state of Fe II is 6D , while most of the observed lines involve the quartet multiplets. Thus, photoexcitation of quartet levels must occur via intercombination transitions which are much weaker than the dipole transitions in low-ionization atomic species where relativistic spin-orbit mixing is weak. This is the case for Fe II, as revealed by inspection of the A-values. We found that photoexcitation of Fe II could not explain the observed relative intensities of optical [Fe II] lines. Nevertheless, recently B96 and Rodríguez (1996) have suggested that [Fe II] lines in Orion are dominated by the fluorescence mechanism. Therefore, further investigation of this issue is necessary.

In terms of the atomic data the present fluorescent excitation model should be quite accurate since we use experimental A-values for most dipole and intercombination transitions. Also, it was shown in BPP that the efficiency of the photoexcitation by UV continuum radiation mechanism drops rapidly with the energy of the odd parity levels, thus the number of energy levels included in the present model should be sufficient. One aspect of the present fluorescent excitation model that was neglected in BPP is the effect of radiative transfer. B96 have suggested that the UV lines dominating the pumping are optically thick and this would affect fluorescent excitation. The line center optical depth for a transition $u - l$, where u and l are the upper and lower levels respectively, is given by

$$d\tau_{ul} = \frac{\pi e^2 \lambda f_{lu}}{mcv} (n_l - n_u g_l / g_u) N_i dr \quad (1)$$

where v is the linewidth ($\sim 13 \times 10^5$ cm s⁻¹ for Orion), g_l and g_u are the statistical weights of the levels, n_l and n_u are the population fractions for the levels, and N_i is the number density of the ion i being considered (Mihalas 1978). In plane parallel geometry the probability that a line photon will escape from the absorption layer is given by

$$P_{esc}(\tau_{ul}) = \frac{1 - e^{-\tau_{ul}}}{\tau_{ul}}. \quad (2)$$

With this expression for the P_{esc} one can compute the emissivity of the lines in NLTE, including the effects of line self-absorption, by replacing the A-values by effective transition probabilities,

$$A'_{ul} = A_{ul}P_{esc}(\tau_{ul}). \quad (3)$$

Here, the total τ_{ul} along the line of sight can be evaluated from eqn. (1) by adopting some reasonable column density of Fe II ions. This column density takes values between 0 at the near side of the cloud and a maximum at the far side of about $N_{Fe\ II} \times r = N_e \times (N(Fe)/N_e) \times (N(Fe^+)/N(Fe)) \times 0.1$ pc $\simeq 8 \times 10^{13}$ cm⁻², where $N_e = 4000$ cm⁻³, $(N(Fe)/N(H)) = 10^{-5.5}$ assuming a depletion factor for iron of ten, and $(N(Fe^+)/N(Fe)) \sim 0.02$. For most of the present calculations we use a mean column density of 4×10^{13} cm⁻². The sensitivity of the results to variations of column density of up to an order of magnitude were also investigated.

To calculate theoretical emissivities and line ratios for the ion it is necessary to simultaneously solve the coupled equations of radiative transfer and statistical equilibrium in an iterative manner. In the present calculations we consider convergence of the level populations to better than 1% for all the levels. This is attained typically after only two or three iterations, since optical depth effects are small and have only marginal importance. The only transitions that can be considered as optically thick, $\tau > 1$, are the dipole allowed transitions that involve the ground state of the ion: $a\ ^6D_{9/2} - z\ ^6D_{9/2}^o$, $a\ ^6D_{9/2} - z\ ^6F_{11/2}^o$, and $a\ ^6D_{9/2} - z\ ^6P_{7/2}^o$. Other transitions, most of them intercombination transitions which

dominate the radiative cascades, exhibit optical depths $\lesssim 0.2$.

We identify particular transitions that are relatively insensitive to fluorescence and which afford reliable density diagnostics. To that end, we compared the population of all 159 levels in our Fe II model for both the collisional and fluorescence models under conditions of $T_e = 10^4$ K and $N_e = 4000$ cm $^{-3}$, and a radiation field as in BPP and Lucy (1995). Then, we identified the levels that are least affected by fluorescence. As expected, among these levels are those with multiplicity two (e.g. $a^2G_{9/2}$ which gives rise to the 7155 and 7452 Å lines), since they are not directly coupled to the sextet ground state. Other levels nearly insensitive to fluorescence are a^6D_J , a^4F_J , a^4D_J , and a^4P_J , which yield all of the IR and the near-IR lines, as well the 8617 and 8892 Å lines.

Emissivity line ratios for lines insensitive to fluorescence are shown in Figs. 4(a)-(c) together with the observed ratios by OTV and Rodríguez (1996). Several other line ratios are shown in Figs. 4(d)-(l). Here, the different curves represent pure collisional excitation, collisional and fluorescence excitation with and without optical depth effects for the radiation field expected in Orion, and fluorescence excitation by a radiation field ten times stronger than in Orion. The observed line ratios are represented by horizontal lines. Also in these figures, the line ratios predicted by the three models of B96 are shown as filled squares.

Several conclusions can be derived from these figures. First, the calculated line ratio curves with and without optical depth effects for the UV lines are nearly indistinguishable. Therefore, optical depth effects under the nebular conditions in Orion have negligible effect on the fluorescent excitation of the optical [Fe II] emission. Secondly, the present results confirm earlier works (e.g. Bautista, Pradhan, & Osterbrock 1994 and BPP) showing that the optical [Fe II] line ratios are consistent with high densities ($10^5 - 10^7$ cm $^{-3}$) regardless of the choice of collision strengths among those currently available. This is particularly

the case for line ratios unaffected by fluorescence, which at $N_e = 4000 \text{ cm}^{-3}$ would yield line ratios different from the observations by more than a factor of two. Among the line ratios that are affected by fluorescence, only a few seem to agree with the observations, while a majority exclude this excitation mechanism. This is also the case for the line ratios considered by Rodríguez (1996), e.g. I(7155)/I(8617) (Fig. 4(c)), I(4287)/I(8617) (Fig. 4(j)), and I(5262)/I(8617) (Fig. 3(b) in BPP and Fig. 4(c) in BP96).

For several of the line ratios (Figs. 4(e-l)) the present model agrees reasonably well with the different models presented by B96. However, their model of Orion entails a mean density for the fully ionized zone (FIZ) of $\sim 10^4 \text{ cm}^{-3}$, which is more than twice the density (4000 cm^{-3} ; OTV) normally derived from [O II] and [S II] line ratios along the line of sight. This has the effect on the model of reducing the depth of the FIZ and the geometrical dilution of the radiation which is inversely proportional to the square of that depth. The higher density in their model should lead also to an overestimation of the optical depths. An unexplained discrepancy between our results and those of B96 appears in the fluorescent pumping of the $4277 \text{ \AA} (a^4F_{7/2} - a^4G_{9/2})$ line. In general, it is found that both our present fluorescent model and those of B96 fail to reproduce the observed line ratios regardless of any possible enhancement of the stellar radiation field.

Rodríguez (1996) compared observed [Fe II] line ratios from 12 different positions in Orion, and from 16 positions in 6 other H II regions, with the ratios expected under collisional excitation conditions. Rodríguez reported considerable scatter for the line ratios and the predictions from BPP’s collisional model. This scatter may be attributed to a variety of causes. One is the combined uncertainties in atomic data and observations. We note that Rodríguez applied the same extinction correction to every spectrum; however, the extinction in Orion is known to vary widely on small spatial scales (e.g. OTV; Pogge et al. 1992; Bautista et al. 1995). In addition, uncertainties from individual line intensity

measurements themselves may be large and should be considered. One particular line that was affected by errors in the atomic data is the 4287 Å line (see previous Section) for which Rodríguez found the largest discrepancies. The new excitation rates for the $a\ ^6S_{5/2}$ upper levels of this line enhance the predicted I(4287)/I(8217) ratio by about a factor of two. Another source of dispersion comes from the fact that a single temperature was assumed in trying to match the observations for twelve different positions in M42 and nine observations of other objects; but the ratios presented are temperature sensitive, particularly at densities of $\sim 10^6\text{ cm}^{-3}$ and higher. For instance, the I(5262)/I(8617) ratio at $N_e=10^6\text{ cm}^{-3}$ varies by more than a factor of two between 5000 and 10000 K (see Fig. 4(c) in BP). One more reason for the observed scatter, and perhaps the most important, is that if the PIZ is a thin transition region it is expected that the physical conditions vary rapidly within it, as suggested in BP95a. Then, a single set of T_e and N_e may not fit all the line ratios simultaneously. Nevertheless, every line ratio reported by Rodríguez indicates electron densities between 10^5 and 10^7 cm^{-3} , while no definitive dependence on fluorescent excitation is found.

Additional spectroscopic evidence against fluorescent excitation of Fe II in Orion is the absence of some allowed emission lines in the observed spectra. If the population of the levels that give rise to the forbidden lines were dominated by cascades from the odd parity levels, the allowed transitions that result from these cascades, some of which lie in the optical region, should be seen. That is the case, for instance, of the 5169.0 Å ($z\ ^6P_{7/2}^o - a\ ^6S_{5/2}$) line that could arise due to the fluorescent excitation of the $^6S_{5/2}$ level, via the sequence $^6D_{9/2} - ^6P_{7/2}^o - ^6S_{5/2}$. Then, the strength of this line should be directly related to the strength of the 4287 Å ($^6S_{5/2} - ^6D_{9/2}$) feature and, under the conditions in Orion, the intensity of the 5169.0 Å line should be about 70% of that at 4287 Å. Other allowed transitions of similar intensity are at 3227.73 Å ($z\ ^4D_{7/2}^o - a\ ^4P_{5/2}$) and 3259.05 Å ($y\ ^4F_{9/2}^o - b\ ^4D_{7/2}$). None of these lines has been observed in Orion.

Moreover, recent echelle observations by Peimbert et al. (1996) establish an upper limit to $I_{Fe II}(\lambda 5169)/I_{[Fe II]}(\lambda 4287)$ of about 0.1, given by the sensitivity limit of their spectra. This indicates that less than 20% of the total intensity of the [Fe II] 4287 Å line in Orion could be explained by fluorescent excitation by UV continuum radiation.

In contrast with Orion and other diffuse H II regions, circumstellar nebulae and the subclass of bipolar planetary nebulae with symbiotic star cores do exhibit rich Fe II spectra, in addition to the forbidden [Fe II] lines, particularly in their core regions, e.g. Eta Carinae (Hamann & DePoy 1994), IRAS 17423-1755 (Riera et al. 1995), He2-25, Th2-B, and 19W32 (Corradi 1995), and M2-9 (Torres-Peimbert & Arrieta 1996). Preliminary comparisons indicate good agreement between our fluorescent model and the observations of these objects (to be reported in a later publication).

3.2. The IR and near-IR [Fe II] lines

The strength of near-IR [Fe II] lines with respect to the optical lines also indicates the presence of high density regions. The 12567 Å ($a^6D_{9/2} - a^4D_{7/2}$) line from Orion was measured by Lowe et al. (1979) using a large circular aperture (2' in diameter) that contains the region studied by OTV. More recently, we also measured this line (Bautista et al. 1995) centered at the same location as OTV, although the effective aperture was only about half of that of OTV. Because of the large changes in local extinction at small scales and the filamentary structure of the low ionization emission of Orion (e.g. Pogge et al. 1992) near-IR to optical line ratios from independent observations covering unequal areas may be unreliable. Nevertheless, B96 used the intensity ratio between the 8617 Å from OTV and the 12567 Å line from Lowe et al. as evidence against the high density regions. This and other ratios of optical lines to the 12567 Å line are shown in Figs. 5(a)-(d). Two sets of observed line ratios are given here according to the 12567 Å intensities from Lowe et al. and

Bautista et al. (about 30% greater). While the I(12567)/I(8617) ratio seems consistent with N_e about 10^4 cm^{-3} , all other optical to near-IR line ratios yield densities greater than 10^5 cm^{-3} . As for the optical line ratios, neither the fluorescent models of B96 nor ours can reproduce the majority of the observed line ratios. Future analysis of IR and near-IR [Fe II] lines is necessary and will need spectroscopic observations of the nebula with sufficiently high resolution to separate most of the [Fe II] lines from the much stronger H I emission.

In conclusion, while the intensity of near-IR lines with respect to the optical lines seems consistent with the existence of high density regions in the Orion nebula, some systematic differences between optical and IR lines may exist, as pointed out in BP95a, and may be indicated by the I(12567)/I(8617) line ratio. Such differences are expected if the PIZ is a thin transition region between the low density, fully ionized medium and the high density neutral medium. Then, the higher excitation optical emission would come preferentially from the highest densities zones, while IR lines, with much lower critical densities, may arise from the more extended lower density gas, as discussed in the next Section.

3.3. Two-zone model of [Fe II] emission

The analysis of optical [Fe II] emission from Orion led to the discovery of high density ($N_e = 10^5 - 10^7 \text{ cm}^{-3}$) PIZ's, but the approximation of a single temperature and density in the emitting region may be responsible for some of the observed dispersion between different line ratios. Moreover, it is possible that some fraction of the lower excitation lines may originate from the FIZ. A more realistic model of the PIZ should take the small scale variations in physical conditions into account. We construct a two-zone model for the [Fe II] emitting region to illustrate how its inhomogeneity could lead to the observed N_e dispersion.

Assuming the dominant [Fe II] optical emission from the PIZ with $(N_e, T_e) = (10^6$

cm^{-3} ; 10,000 K), 50% of the gas ionized, and nearly all iron as Fe^+ , the intensity of the 4277 Å line, for instance, with respect to $\text{H}\beta$, may be expressed as

$$\frac{I_{[\text{Fe II}]}(4277)}{I_{\text{H}\beta}} = \frac{j(4277)}{j(\text{H}\beta)} \frac{N_{\text{PIZ}}(\text{Fe}^+) l_{\text{PIZ}}}{N_{\text{FIZ}}(\text{H}^+) l_{\text{FIZ}}}, \quad (4)$$

where j is the absolute emissivity of the line per ion, N_{PIZ} and N_{FIZ} indicate densities in the PIZ and FIZ respectively, and $l_{\text{PIZ}}/l_{\text{FIZ}}$ is the mean ratio of the column lengths of the two media. From the measured intensity of the 4277 Å line with respect to $\text{H}\beta$, equal to 4.3×10^{-4} (OTV), and the FIZ density of 4000 cm^{-3} , the ratio of the depths of the PIZ and FIZ is of the order

$$\frac{l_{\text{PIZ}}}{l_{\text{FIZ}}} = 10^{-6} - 10^{-7}. \quad (5)$$

Thus, the PIZ appears to be a very thin region compared with the extent of both the FIZ and the ionization-dissociation front. As a consequence, a very small fraction of Fe^+ in the FIZ could be sufficient to dominate the emission of lines with low critical densities. For instance, for the 12567 Å line, with a critical density of the order of 10^4 cm^{-3} , an increase in N_e from 4000 to 10^6 cm^{-3} enhances its emissivity by a factor of only 10.4, much less than the factor of ~ 250 for the optical lines. Therefore, even if only $\sim 2\%$ of the iron in the FIZ is in Fe^+ , one can express the intensity of this line by

$$I(12567) = (j(12567)N(\text{Fe}^+)l)_{\text{FIZ}} + (j(12567)N(\text{Fe}^+)l)_{\text{PIZ}}, \quad (6)$$

to obtain $I(12567) = (j(12567)N(\text{Fe}^+)l)_{\text{FIZ}} \times (1 + 0.1)$, (i.e. with the contribution of the PIZ about one tenth that of the FIZ). The 12567 Å line, and the IR and near-IR lines with similarly low critical densities, should originate preferentially from the FIZ, unlike the optical lines. Two predictions may be made from such a scenario: (1) line density diagnostics with IR lines may behave differently than those with optical lines and would be consistent with the conditions of the FIZ, e.g. $(N_e, T_e) \approx (4000 \text{ cm}^{-3}, 9000 \text{ K})$; (2) there should be clear kinematic differences between the IR and optical lines, i.e. the velocities

measured from the IR [Fe II] lines should be similar to those of the nebular [S II] emission, unlike the velocities from optical [Fe II] lines which are close to those of [O I] at the ionization front (see Section 4).

Table 5 shows the relative intensities of the optical and near-IR lines calculated with a model that combines a FIZ and a thin high density PIZ. The conditions in the FIZ are: $(T_e, N_e) = (9000 \text{ K}, 4000 \text{ cm}^{-3})$, a thickness of 0.13 pc, and Fe⁺ ionization fraction of 2%; and the conditions in the PIZ are: $(T_e, N_e) = (10000 \text{ K}, 2 \times 10^6 \text{ cm}^{-3})$, thickness of 3×10^{-8} pc, and Fe⁺ ionization fraction of 80%. Fluorescent excitation for conditions similar to those of Orion is also included. This mechanism may only affect the emission from the FIZ where the electron density is lower than the critical density for fluorescence. The present results are also compared with observations of Orion by OTV, and with the models by B96. The percentage contribution of the PIZ to the total intensity of each line for models (I) and (II) are indicated within brackets. Also, the mean dispersion between OTV’s observations and each of the models is given at the bottom of the table for the lines in common with B96.

Table 5 shows that the observed optical and near-IR spectra can be reasonably well explained by this simple two-zone model, while serious discrepancies exist when the contribution from the PIZ is neglected. For instance, it can be seen that the observed intensity of the $\lambda 5262$ line with respect to the $\lambda 8617$ differs by factors of two to three from theoretical models that neglect the PIZ (present model III and models A, B, C of B96). This ratio is one of the ratios considered by Rodríguez (1996). On the other hand, by including the contribution of a thin high density PIZ (present models I and II) good agreement is found for most lines including the near-IR lines. The mean dispersions (σ) between observations and the various models are also indicated in Table 5. This also shows that the models presented here are in much better agreement with the observations than those of B96 et al. Moreover, model (II) of Table 5 that neglects fluorescent excitation in

the FIZ seems to be better than model (I). This may suggest that the UV continuum flux considered in (I), as suggested by Lucy (1995), is overestimated. On the other hand, model (III) and models (A), (B), and (C) of B96, which neglect the contributions from the high density zone differ from the observed line ratios by 53-80%. Notice also that in models (I) and (II) which best fit the observations the contributions of the PIZ dominate the total intensity of the optical lines, particularly in model (II) where the PIZ is responsible for 70-80% of the optical emission. A better representation of the [Fe II] nebular emission would require radiative and hydrodynamic modeling of the structure of the PIZ, which exceeds the capabilities of current photoionization modeling codes.

3.4. The [Fe III] lines

Forbidden [Fe III] lines are expected to be collisionally excited. Fluorescent pumping of these lines by continuum radiation is unlikely because of the large energy difference (more than 1 Ry) between the 5D ground state of the ion and the first odd parity levels. Moreover, the stellar continuum radiation in this energy range is absorbed for the most part by hydrogen.

We use a 34-level CR model for Fe III with collision strengths from Zhang (1996) and transition probabilities from Nahar & Pradhan (1996). An energy level diagram for the Fe III system is shown in Fig. 6, where the most important lines under nebular conditions in the optical and near-IR regions are indicated. One interesting characteristic of the Fe III system is that the near-IR emission originates from higher excitation levels (3G_J) than the optical lines (levels 3F_J , 3H_J , and 3P_J), which explains why the near-IR [Fe III] emission is usually very weak in gaseous nebulae. Also, the maximum energy difference between the levels that give rise to the optical lines is only about 0.02 Ry (~ 3000 K), which makes the relative line intensities of these lines insensitive to small temperature variations.

Selected line ratios among optical and near-IR lines are shown in Figs. 7(a)-(j) at $T_e = 9000$ K. Optical observations of Orion are from OTV, Greve et al. (1994), and Rodríguez (1996) and near-IR observations are from DePoy & Pogge (1994) and Bautista et al. (1995). The observation by Greve et al. and Rodríguez include several different positions; here we present the entire ranges of their measured line ratios. The observed [Fe III] line ratios in Orion agree well with the diagnostics using lines of other species, such as [S II], that indicate N_e of a few times $\times 10^3 \text{ cm}^{-3}$. The observations by Greve et al. indicate densities between a few times 10^3 to almost 10^4 cm^{-3} , with the lowest N_e near the Trapezium and highest towards the edges of the nebula. The observations of Greve et al. also reveal variations in the intensities of the [Fe III] lines with respect to $H\beta$ along six consecutive positions on a North-to-South line centered at $\sim 20'$ W of Θ^1 Ori A. Here, the intensity of the [Fe III] emission seems to have a minimum near the Trapezium region and increases toward the edges of the nebula, particularly in towards the North. This behavior seems correlated with the [N II] and [O II] emission, but it is anti-correlated with the intensity of the He I, [O III], [S III], and [Ne III] lines. These correlations between the [Fe III] emission and the low ionization species, and the anti-correlation with higher ionization ions, are consistent with a drop in the ionization of the plasma towards the edges of the nebula.

3.5. The [Fe IV] lines

We use a 33-level CR model of Fe IV that includes the collisional rate coefficients from Zhang & Pradhan (1997) and A-values from Garstang (1958). An energy level diagram for the Fe IV system is shown in Fig. 8, which illustrates the lowest metastable levels 4G_J , 4P_J , and 4D_J that give rise to lines in the UV. Emission lines in the optical from higher excitation levels, about 0.5 Ry (~ 6.8 eV) above the ground state, are expected to be weak unless relatively high densities and/or temperatures are present. Fluorescent excitation

by stellar continuum seems unlikely, as photons with energies higher than 1.7 Ry (~ 23 eV) are required to excite the lowest odd parity levels. We identify the strongest [Fe IV] transitions for conditions of $N_e = 4000 \text{ cm}^{-3}$ and $T_e = 9000 \text{ K}$. These UV transitions, in decreasing order of intensity, are: 2835.7 Å (${}^6S_{5/2} - {}^4P_{5/2}$), 2829.4 Å (${}^6S_{5/2} - {}^4P_{3/2}$), 2567.6 Å (${}^6S_{5/2} - {}^4D_{5/2}$), 2567.4 Å (${}^6S_{5/2} - {}^4D_{3/2}$), and 3101.7 Å (${}^6S_{5/2} - {}^4G_{11/2}$). The 3101.7 Å line stems from the first excited metastable level ${}^4G_{11/2}$, with a transition probability to the ground level of only $\sim 10^{-5} \text{ s}^{-1}$; yet, it may be observable and valuable in understanding the excitation mechanisms for Fe IV.

Recently, the detection of the [Fe IV] 2835.7 Å line in Orion was reported by Rubin et al. (1997) using the GHRS/HST spectrograph. Based on the observed 2835.7 Å line and their models, Rubin et al. derived the Fe/H abundance ratio in Orion to be lower than the solar by a factor between 70 and 200, much lower than any previous estimate from [FeIII] or [FeII] lines. A reexamination of this result is presented in Section 5.

In the optical region the strongest [Fe IV] features are those at 4906.6 Å (${}^4G_{11/2} - {}^4F_{9/2}$), 4900.0 Å (${}^4G_{9/2} - {}^4F_{7/2}$), 4903.1 Å (${}^4G_{7/2} - {}^4F_{7/2}$), 4198.2 Å (${}^4G_{11/2} - {}^2H_{9/2}$), and 4152.3 Å (${}^4G_{9/2} - {}^2H_{11/2}$). However, the strength of the 4906.6 Å line with respect to the 2835.7 UV feature is only about 0.014. Similarly, the strength of the 4906.6 Å line with respect to the nearby [Fe III] 4881 Å line is about $0.012 \times N(\text{Fe}^{3+})/N(\text{Fe}^{2+})$. These [Fe IV] features may be detectable with modern instruments. Some potentially useful N_e and T_e sensitive UV and optical line ratios are shown in Figs. 9(a)-(h).

Surprisingly, strong optical [Fe IV] emission is seen in planetary nebulae with symbiotic cores like M2-9 (Balick 1989; Torres-Peimbert & Arrieta 1996). The reason for this seems to be the high N_e ($\sim 10^7 \text{ cm}^{-3}$) in the nebular core. Fig. 10 compares the density diagnostic results from [Fe IV] and [O III] lines as measured by Torres-Peimbert & Arrieta. The very good agreement between both diagnostics provides observational support for the accuracy

of the atomic data and the present excitation model for Fe IV.

4. [O I] Diagnostics

In the optical region of the spectrum there are three collisionally excited [O I] lines sometimes detected in H II regions; these are due to the transitions $^1D_2 - ^3P_1$, $^1D_2 - ^3P_2$, and $^1S_0 - ^1D_2$ at $\lambda\lambda$ 6363, 6300, and 5577 respectively. All three lines were reported by OTV, and Baldwin et al. (1991) at twenty one different positions in Orion. These observations were used by BP95a to diagnose the physical conditions in the [OI] emitting regions, which were found to be in good agreement to those for optical [FeII]. BP95a also recognized that the [OI] observations may suffer to varying degrees from night sky contamination, so an uncertainty of about a factor of two on the line ratios was assumed.

Recently, B96 carried out observations of the [O I] emission from Orion using the *Faint Object Spectrograph* (FOS) on the *Hubble Space Telescope* (HST) and Cassegrain echelle spectrograph on the 4 m telescope of the *Cerro Tololo Inter-American Observatory* (CTIO). B96 report no detection of the [O I] 5577 Å line, for a position in Orion quite distant from that of OTV. B96 suggest that previous measurements of the [O I] 5577 Å line were contaminated by telluric emission and did not represent actual emission from Orion. Their observations establish lower limits to the $I(6300+6363)/I(5577)$ ratio that differ by up to nearly a factor of four from the measurements of OTV and Baldwin et al. (1991). The HST and CTIO measurements of B96 establish upper limits of 10^6 and $2 \times 10^5 \text{ cm}^{-3}$ to the averaged electron density of the emitting region assuming $T_e = 10^4$ K. If temperatures of 9000 or 8000 K were adopted instead, the N_e upper bounds would be $9 \times 10^5 \text{ cm}^{-3}$ (HST), $3 \times 10^5 \text{ cm}^{-3}$ (CTIO), and $2 \times 10^7 \text{ cm}^{-3}$ (HST), $5 \times 10^6 \text{ cm}^{-3}$ (CTIO) respectively. This is illustrated in Fig. 11.

It is important to note that the temperature diagnostic from [NII] lines given by B96 is inapplicable to the [OI] region because [NII] and [OI] are emitted by different regions; NII requires photon energies of about 14.5 eV which is higher than the formation energy of OII (see next section). Reliable observations of optical [OI] and [FeII] lines from the same position in the nebula would be valuable in constraining the mean temperature of the PIZ.

5. Kinematic Analysis of the Orion Nebula

Although photoionization models generally assume static conditions, the differential expansion of nebulae is known. For example, Kaler (1967) presented radial velocities for a variety of ions taken from spectroscopic observations of Orion by Kaler, Aller, & Bowen (1965). This study includes the expansion velocity of Fe^+ obtained from [Fe II] lines. Fehrenbach (1977) reported additional measurements of three different positions in Orion which included the velocities from forbidden emission of Fe II, Ni II, and S II. It was pointed out in this work that there is a large separation in expansion velocity between these low ionization species and the higher ionization ions, e.g. H^+ and O^{2+} . The most recent kinematic studies of Orion have been presented in several papers by Castañeda, O’Dell, and Wen. In particular, O’Dell & Wen (1992) measure the expansion velocities with the [O I] $\lambda 6300$ Å line for several arcminutes across the core of the nebula. Fig. 12 shows the measured expansion velocities of various ions from Kaler (1967), Fehrenbach (1977), and O’Dell & Wen (1992) against the energy necessary to form them. This figure is adapted from plots previously presented by Kaler (1967) and Balick, Gammon, & Hjellming (1974). The ordinate on the right represents the observed velocities in the heliocentric system, and the ordinate on the left gives the velocities with respect to the molecules in the OMC-1 cloud core ($+27 \text{ km s}^{-1}$). The data by Fehrenbach correspond to the position GA417 in Table 3 of his paper. One difficulty with these data is that only statistical dispersions for the

mean velocities are given, without including the instrumental errors which dominate when the number of lines observed is small. We have estimated error bars for these measurements by taking the ratio of the instrumental error ($\sim 3 \text{ km s}^{-1}$) divided by the square root of the number of lines measured. The data from O’Dell & Wen correspond to that given in Table 5 of their paper which includes measurements by O’Dell et al. (1991) and Castañeda (1988).

Figure 12 shows a strong dependence of the velocities of the ions on their formation energies. In particular, there is a sharp division in velocity between ions that require photon energies greater than 13.6 eV (1 Ry), indicated by the vertical dashed line, and neutrals and ions with lower first ionization potentials, such as O^0 , Fe^+ , and Ni^+ . This velocity stratification in Orion was previously pointed out by several authors, e.g. Kaler (1967) and Balick et al. (1974). It is also clear from the figure that forbidden emission from O I, Fe II, and Ni II should stem mostly from the same PIZ at the ionization front, as predicted by photoionization models (B96) and seen from the $[\text{O I}]/[\text{Fe II}]$ and the $[\text{Ni II}]/[\text{Fe II}]$ correlations (BP95; BPP). The velocities associated with $[\text{S II}]$ emission, on the other hand, lie in between those of the ionization front and the fully ionized zone. This is because, although S^+ requires only 10.4 eV to be created, it can survive to photons up to 23.3 eV. By contrast, Fe^+ ionizes to Fe^{++} at 16.2 eV and, in addition, Fe^+ ionizes to Fe^{++} by charge exchange with H^+ (Neufeld & Dalgarno 1987). Furthermore, spectroscopic diagnostics from $[\text{S II}]$ should mostly sample the region in the FIZ right behind the ionization front, and may not agree with the results from $[\text{Fe II}]$ lines.

Fig. 12 also shows that the velocities of species in the PIZ are similar to those of the photodissociation region (PDR) and the molecular cloud. This has implications for constraining the gas densities in that zone. The continuity equation for the flow co-moving with the ionization front implies that any two points along the gas flow with similar bulk velocities should have about the same density, as in the case of the PIZ, the PDR, and

molecular cloud. From the mass conservation equation in the frame of reference comoving with the ionization front $\rho v = \text{constant}$. Then, one can establish limits on the density of the PIZ by estimating the velocity of the ionization front from known densities and velocities of the PDR and, for instance, the [O II] emitting zone. Thus,

$$(10^5 \text{cm}^{-3}) \times (26.1 \text{kms}^{-1} - u_s) = (4000 \text{cm}^{-3}) \times (13.8 \text{kms}^{-1} - u_s) \quad (7)$$

yields a heliocentric velocity for the ionization front of about 26.6 km s^{-1} . From this we have

$$\rho_{PIZ} = 10^5 \text{cm}^{-3} \times \frac{(26.1 \text{kms}^{-1} - 26.6 \text{kms}^{-1})}{((25.8 \pm 0.6) \text{kms}^{-1} - 26.4 \text{kms}^{-1})} \geq 4 \times 10^4 \text{cm}^{-3}, \quad (8)$$

where 10^5 cm^{-3} is the estimated density of the PDR (Tielens & Hollenbach 1985) and 26.1 km s^{-1} is the flux averaged velocity of the PDR measured from radio CII emission (Goudis 1982). Therefore, the averaged density of the [O I], [Fe II], [Ni II] emitting zone should be at least ten times greater than that at the [O II] region (FIZ). No upper limit on the density of the PIZ can be obtained given the present uncertainties in the expansion velocities.

Apart from Orion, other H II regions (M43, M8, M16, M17, M20, and NGC7635 observed by Rodríguez 1996) also show high density PIZ's. It is, then, natural to ask: How do warm, high density PIZ's form? The answer may be found in hydrodynamic models of ionization fronts, such as those of Tenorio-Tagle (1977), Bedijn & Tenorio-Tagle (1981) and García-Segura & Franco (1996). Tenorio-Tagle and Bedijn & Tenorio-Tagle showed that I-fronts propagating into dense clouds are neither smooth nor in pressure equilibrium with the ambient gas. Rather, the I-front and the leading shock can give rise to highly compressed regions due to the so-called 'rocket-effect'. The density and pressure of these regions can be orders of magnitude above those of the undisturbed gas. Moreover, these regions dissipate and reform as they become fully ionized and the shock travels into the molecular cloud. In their recent three-dimensional simulation of the forming H II regions, García-Segura & Franco (1996) also found that high density regions should form within

I-fronts with a shell-like structure at the interface between the H II region and the dense molecular cloud. The densities of these shells may lead to instabilities, yielding ‘elephant trunks’ and rim-like structures.

6. Photoionization Modeling of Orion

The new atomic data for Fe I–V enable an accurate calculation of the ionization structure of Fe in low ionization nebulae. Iron has only a minor effect on the cooling of the fully ionized region, thus changes in the ionization of iron should not alter the conditions in the nebula. Therefore, one can compute the temperature, electron density, and ionizing radiation flux at every point in the nebula using presently available photoionization modeling codes, and then use these results to calculate the ionization-recombination balance of iron separately.

6.1. Fe Ionization Balance

We use the computer code CLOUDY (Ferland 1993) for photoionization modeling, but incorporate the new atomic data for the Fe ions (Table 1). Stellar continuum radiation, dust content, and turbulence velocities were similar to those in Baldwin et al. (1991). We assume mean chemical abundances for the Orion nebula as in Ferland (1993), which are based on results from Baldwin et al., OTV, and Rubin et al. (1991a). We further assume constant total (gas and radiation) pressure and a mean density throughout the cloud of $\sim 10^4 \text{ cm}^{-3}$. This model allows us to study the effects that the new atomic data have on the calculated ionization structure of iron in the nebula. However, as shown later, this model seems unable to reproduce the observed spectra of high and low ionization species simultaneously with the observed depth of the ionized region.

In Fig. 13 we show the physical conditions (N , T_e , N_e) in the cloud, as obtained from the model. In Fig. 14 we present examples of the ionizing radiation flux at two different zones in the cloud (a) at the near side to the ionizing star (Θ^1 Ori C, spectral type O7; Conti & Alschuler 1971) and (b) near the ionization front. The ionization thresholds of Fe I–III marked in Fig. 14 reveal the correlation with the photoionization cross sections in Fig. 1, near the ionization thresholds as they affect the total photoionization rate. For instance, in the photoionization of Fe I the ionizing flux per photon energy unit is maximum between its ionization threshold ~ 0.55 Ry (7.5 eV) and 1 Ry (13.6 eV), beyond which most of the photons are absorbed by H I ionization. This is the same energy interval for which the previous photoionization data (RM, Verner et al. 1993) underestimates the Fe I cross section by up to three orders of magnitude (Fig. 1). A similar situation applies to Fe II whose ionization potential (1.18 Ry) lies below that of neutral He (1.81 Ry). As one goes deeper in the cloud, fewer photons with energies greater than 1.81 Ry are available and the photoionization of Fe II is dominated by the flux in the near threshold region, where it is heavily attenuated by extensive resonance structures (Fig. 1).

We calculate the photoionization rate of Fe I–IV by integrating the new photoionization cross sections over the ionizing flux at every point in the nebula. At high photon energies where the R-matrix data is not available, we use the central field data by RM which should be reasonably reliable at high energies, as seen by the relatively small differences with the close-coupling results (Fig. 1). Photoionization from excited states of Fe ions was found to be negligible and was not considered.

Fig. 15 shows our results for the photoionization rates as a function of distance from the ionizing star (Θ^1 Ori C), compared with those obtained using the cross sections of RM. It is seen that the ionization rates for Fe I–III calculated with the new data increase by nearly a factor of two for Fe I and Fe II, and about a factor of five for Fe III with respect

to those found using cross sections of RM. Near the ionization front the photoionization rates using the new data are about an order of magnitude larger than those using RM. This is because deeper in the cloud the ionization becomes dominated by photons below the ionization thresholds of H I for Fe I, and of He I for Fe II, where the discrepancies between the two sets of cross sections are greater. We emphasized that the resonance structures are physical features and their effect on the photoionization cross section should be taken into account, and that there can be a significant loss of accuracy in using fits of only the background cross sections.

The effect of charge exchange on Fe ions also needs to be considered, particularly



The rate coefficients for these reactions were calculated by Neufeld and Dalgarno (1987) using the Landau-Zener approximation and might be highly uncertain for complex atomic systems such as the Fe ions. This is therefore the main source of uncertainty for the Fe II/Fe III ionization balance as far as the atomic data is concerned. For example, changes in the rates by the estimated uncertainty of a factor of three varies the ionic fractions of Fe I and Fe II by up to 20% (Fe III and Fe IV remain almost unaffected). However, the uncertainties in the rates could be much higher than a factor of three, and new calculations or experimental measurements are needed. Charge exchange ionization and recombination involving Fe^+ and Fe^{++} are very important in limiting the physical extent of the FeII emitting region.

Fig. 16 shows our results for the ionization fractions of Fe I-IV in the nebula, compared with those with earlier atomic data in CLOUDY, which uses the RM cross sections extrapolated to the ionization threshold. For Fe III for example, CLOUDY includes a value for the cross section at 2.2 Ry of 8.8 Mb which is about four times higher than the background cross section from the new data (Nahar 1996a). This overestimation of the

cross section compensates in part for the missing contribution of the resonance structures. In addition, the code uses recombination coefficients from Woods et al. (1981) which are about a factor of two too low at T_e around 10^4 K. Therefore the agreement between the CLOUDY predictions and the present results is somewhat fortuitous.

6.2. Modeling of Fe in Orion

Apart from the atomic data, the main source of uncertainty in calculating the ionization structure of Fe in nebulae is the assumed structure for the cloud. Different assumptions about the radial density dependence (constant, exponential, or power law), or constant thermal and/or radiative pressure, constant temperature, etc. result in significant differences in the ionization structure of Fe and other ions. For instance, Baldwin et al. (1991) assumed a mean gas density for Orion of $\sim 10^4 \text{ cm}^{-3}$, and constant gas pressure, and obtained Fe ionic fractions averaged over line-of-sight of $(\text{Fe}^+/\text{Fe}^{2+}/\text{Fe}^{3+}) = (0.01/0.24/0.74)$. On the other hand, Rubin et al. (1991b) used an exponential density profile, as a function of radius, up to a maximum of 5000 cm^{-3} and a “plateau” beyond, to obtain $(0.05/0.41/0.53)$. Some differences between these two models for the ionic fractions of other elements are also present, e.g. He. One might therefore expect an uncertainty of about a factor of five in an iron abundance estimate based on [Fe II] lines and ionization corrections from photoionization models. If [Fe III] lines are used instead, the uncertainty would be about a factor of two. Rubin et al. (1997) have recently estimated the iron abundance in Orion from [Fe IV] lines and obtained values that differ by nearly a factor of three from those of Baldwin et al. and Rubin et al. (1991b).

Another difficulty with modeling the ionization structure of iron, and particularly the ionic fraction of Fe^+ , is the inadequacy of the physics of ionization fronts in photoionization models that assume static conditions everywhere in the cloud, with the ionization front at

a distance where all ionizing photons have been absorbed. However, real photoionization fronts are highly dynamic and more realistic models of ‘blister’ H II regions, like Orion, should consider the effect of ionization fronts where enough ionizing photons are available to photoionize new neutral material. One should also take into account the radiation energy that accelerates the gas away from the ionization front into the fully ionized zone. This difficulty with the thickness of the cloud and the location of the ionization front is readily noticed by comparing the Rubin et al. (1991a) and the Baldwin et al. models. The model of Rubin et al. uses an exponentially increasing gas density with a peak value of 5000 cm^{-3} and predicts a distance to the He ionization front of 0.277 pc. By contrast, the estimated mean thickness of the emitting region from the surface brightness of the $\text{H}\alpha$ emission is only 0.13 pc (Wen & O’Dell 1995). Perhaps, the extent of the ionized region in the Rubin et al. model could be reduced by decreasing the number of ionizing photons in the model (Q), but this would conflict with direct measurements of Q -values from radio continuum flux density. The Baldwin et al. model, on the other hand, gives a thickness for the ionized region of about 0.07 pc, closer to observations, but the adopted density is $\sim 10^4 \text{ cm}^{-3}$. Such a density is considerably higher than what is observed over most of the nebula except for a region immediately south-southwest of the Trapezium. If a lower density had been adopted, like that in Rubin et al., a much thicker ionized zone would have been obtained.

In modeling the ionization structure of Orion we constructed a simple model of the nebula that uses a constant density of 4000 cm^{-3} , based on long established [S II] and [O II] line diagnostics, up to a maximum distance from the star where a high density ionization front is encountered. The position of the front is optimized to match the observed relative intensity of the [O I] 6300 Å line with respect to $\text{H}\beta$ without significantly affecting the intensities of [O II] and [O III] lines. Two models were calculated for peak particle densities of the ionization front of 10^6 cm^{-3} and 10^7 cm^{-3} . Other conditions such as turbulent velocity, stellar temperature, and number of ionizing photons are as in Baldwin et

al. (1991). There is no explicit control over the electron density, temperature, and depth of the PIZ, and they are calculated in the model according to photoionization-recombination equilibrium which depends only on the particle density and position of the ionization front. Table 5 shows the results, together with three different sets of observations, columns 3-5, from OTV, B96, and Greve et al. (1994). The results reported by B96 are shown in columns 6-8. The results for five different models calculated here, (I) to (V), are given in columns 9-13.

Inspection of Table 5 reveals the difficulty in reproducing the observed spectrum with current photoionization models and, in particular, the problems in trying to simultaneously match all of the observed ionization stages of a given element, e.g. oxygen. Model (I) in the present work was calculated assuming constant gas pressure conditions with a mean density of $\sim 10^4 \text{ cm}^{-3}$, as in B96. The models systematically overestimate the intensity of [O II] and [O III] from a few percent to over a factor of two. On the other hand the [O I] emission is underestimated by up to a factor of three. Models (II) and (III) were calculated with constant gas pressure conditions but with a mean density of $\sim 4000 \text{ cm}^{-3}$ determined by the spectroscopic diagnostics. The difference between models (II) and (III) is that the former uses the LTE stellar continuum flux from Kurucz (1979), while model (III) uses a NLTE stellar continuum from Sellmaier et al. (1996). Clearly, adopting a lower density for the cloud and the use of accurate NLTE stellar continuum fluxes improves the results for [O II] and [O III] emission with respect to observations. However, the discrepancies for the [O I] lines increase to about a factor of five or more. This is because lowering the mean density increases the ionization, reducing the fractions of neutrals. The same conditions as in model (III) were used for (IV) and (V), together with high density ionization fronts in the PIZ. Model (IV) uses a front with peak density 10^6 cm^{-3} at a depth in the cloud of $6.5 \times 10^{17} \text{ cm}$ ($= 0.21 \text{ pc}$), and model (V) has a front with peak density 10^7 cm^{-3} at a depth of $6.9 \times 10^{17} \text{ cm}$ ($= 0.22 \text{ pc}$). [O II] and [O III] lines in both of these models remain nearly

unaltered with respect to model (IV) and are in reasonable agreement with observations. However, the [O I] lines are considerably enhanced, close to the observed levels, as a result of the contribution from the PIZ. In these models the mean temperatures and hydrogen ionization fractions, $N(\text{H}^+)/N(\text{H})$, are 8700 K and 0.49 respectively for model (IV), and 8200 K and 0.31 for model (V).

Table 6 clearly shows the effect of the assumed density structure of the cloud on the predicted spectrum from photoionization modeling. The table also shows that there is a significant contribution to the emission from neutral and low ionization species from the high density PIZ. It must be pointed out, however, that the models presented in Table 6 are still illustrative, and accurate modeling of ionization fronts requires a radiative-hydrodynamic treatment.

7. The Iron Abundance in Orion

There are two basic approaches typically used to estimate gas phase abundances in gaseous nebulae. The first one consists of estimating the ionic abundances, normally relative to hydrogen, directly from spectra assuming mean density and temperature derived from line ratio diagnostics. Then, the abundances of all observed ions of the same element are added to yield the total gas phase abundance of the element. Few prior assumptions need to be made about the structure of the cloud, but the method has the disadvantage that it neglects any temperature and density variations along the line of sight, as predicted from photoionization models (e.g. Fig. 13). Additional temperature fluctuations, different from photoionization models, have also been studied by Peimbert (1967; 1995, and references therein). The second approach consists of photoionization modeling to reproduce the conditions in the cloud, and the abundance of elements adjusted to match the observed spectrum. The results depend on the initial assumptions about the structure of the nebulae

and may be subject to uncertainties in the model. Relative ionic abundances should be most accurate when calculated for ions that co-exist and whose lines are produced by the same mechanism, e.g. collisional excitation or recombination. Lines excited by fluorescence are difficult to interpret as they generally involve a large number of levels and depend on the nebular photoexcitation emission.

For Orion we calculate the abundances of Fe^+ , Fe^{2+} , and Fe^{3+} relative to O^0 , O^+ , and O^{2+} respectively, and derive the total $\text{N}(\text{Fe})/\text{N}(\text{O})$ from each of the ionic ratios using calculated ionic fractions. The abundance ratio $\text{N}(\text{Fe}^{i+})/\text{N}(\text{O}^{j+})$ can be obtained from the observed line intensities 'I', and the calculated emissivities 'j', as

$$\frac{N(\text{Fe}^{i+})}{N(\text{O}^{j+})} = \frac{I_{\text{Fe}^{i+}}}{I_{\text{O}^{j+}}} \times \frac{j_{\text{O}^{j+}}}{j_{\text{Fe}^{i+}}}. \quad (10)$$

The total $\text{N}(\text{Fe})/\text{N}(\text{O})$ abundance ratio is

$$\frac{N(\text{Fe})}{N(\text{O})} = \frac{N(\text{Fe}^{i+})}{N(\text{O}^{j+})} \times \frac{X(\text{O}^{j+})}{X(\text{Fe}^{i+})}, \quad (11)$$

where X is the calculated ionic fraction in the nebula.

We first calculate the $\text{N}(\text{Fe}^+)/\text{N}(\text{O}^0)$ ratio from the intensity ratio measured by OTV, $I_{\text{Fe}^+}(\lambda 8617)/I_{\text{O}^0}(\lambda 6300) = 0.069$. The particular advantage of ratios of the optical [Fe II] lines and the [O I] 6300 line is that the excitation energies are similar, as are the critical densities $> 10^7 \text{ cm}^{-3}$. These ratios are therefore insensitive to uncertainties in T_e and N_e . If one takes a density for the emitting region of 10^6 cm^{-3} one gets $\text{N}(\text{Fe}^+)/\text{N}(\text{O}^0) = 0.069 \times 1.08 = 0.075$. If an electron density of 4000 cm^{-3} were adopted instead, the abundance ratio would be $\text{N}(\text{Fe}^+)/\text{N}(\text{O}^0) = 0.069 \times 0.80 = 0.055$, which differs by less than 30% from the previous value. Similar results can be obtained using other optical [Fe II] lines. A calculation of the total $\text{N}(\text{Fe})/\text{N}(\text{O})$ ratio from Fe^+ and O^0 depends on the ionic fractions. If most of the emission emerges from the PIZ, where Fe^+ and O^0 are the dominant ionization stages, the ratio of the ionic fractions would be about unity and the $\text{N}(\text{Fe})/\text{N}(\text{O})$ ratio (as

derived in BP95a and BPP) should be close to the solar value of 0.048 (Aller 1987) or 0.044 (Seaton et al. 1994). If the emission originated mainly from the FIZ the ratios are 0.16, 0.27, 0.35 respectively, from photoionization models from the present work (Model III), Baldwin et al. (1991), and Rubin et al. (1991a; 1991b). This yields lower bounds to the total $N(\text{Fe})/N(\text{O})$ between $\sim 1/4$ and $1/2$ of the solar value.

Fe^{2+} and O^+ are expected to be mostly coexisting; one can therefore calculate $\text{Fe}^{2+}/\text{O}^+$ with good accuracy. In Fig. 17 we plot this abundance ratio as a function of electron temperature and density. This was calculated according to Eq. (10) using line intensity ratios from OTV for $I_{\text{Fe}^{2+}}(\lambda 4881)$ and $I_{\text{O}^+}(\lambda 3728)$ (solid curves), and $I_{\text{O}^+}(\lambda 7322)$ (dashed curves). In principle, one should obtain the same relative abundance ratio from every line, thus the actual conditions of the emitting region and the abundance ratio are given by the point where the different curves intersect. In that sense, Fig. 17 shows that if the temperature of the region were 9000 K, the electron density should be about 2500 cm^{-3} . Similarly, a density of 4000 cm^{-3} , as adopted by OTV, would yield a temperature close to 7000 K. We adopt mean conditions for the Fe^{2+} and O^+ emitting region of $N_e = 3000 \text{ cm}^{-3}$ and $T_e = 8000 \text{ K}$. Table 7 presents the abundance ratios derived from individual [Fe III] lines observed in Orion by OTV. The mean abundance ratio is $N(\text{Fe}^{2+})/N(\text{O}^+) = 0.011 \pm 0.003$, where the error comes from the statistical dispersion (the value from the blend of lines at 4986 \AA was excluded since it is more than two sigma away from the mean). The ratio of the ionic fractions, $X(\text{O}^+)/X(\text{Fe}^{2+})$, according to any of our present models (III), (IV), or (V), is about 1.1, which yields an iron to oxygen abundance ratio by number of about 0.012 ± 0.003 or $1/(3.7 \pm 1.0)$ of the solar value. Notice that the ratio of the ionic fractions from the models of Baldwin et al. (1991) and Rubin et al. (1991a; 1991b) are higher than the present value, 1.75 and 1.39 respectively, and they would yield abundance ratios of about half to 65% solar.

The iron to oxygen abundance ratio in the Fe IV emitting region can be calculated from the [Fe IV] and [O III] lines. We use the intensity of the [Fe IV] 2827 Å line with respect to H β , as measured by Rubin et al. (1997), and OTV’s observations of [O III] lines also with respect to H β . Fig. 18 shows the calculated $N(Fe^{3+})/N(O^{2+})$ abundance ratios as a function of temperature for several values of N_e . Here the solid curve represents the abundance ratio from the [O III] 4363 Å line and the dashed curve indicates the ratio obtained with the [O III] 4959 Å feature. As before, T_e , N_e , and the abundance ratio are given by the crossing points of the two curves. We find the conditions for the Fe $^{3+}$ - O $^{2+}$ emitting region are about $T_e = 10500$ K and $N_e = 4000$ cm $^{-3}$, with a $N(Fe^{3+})/N(O^{2+})$ abundance ratio of 0.002. The uncertainty in this value from errors in the assumed conditions is less than 10%, as seen from Fig. 18. The $X(O^{2+})/X(Fe^{3+})$ ionic fractions ratio from our present model (III), (IV), or (V) is 0.96, which yields a total $N(Fe)/N(O)$ of 0.0017 or 1/26 of the solar value. If ionic fractions from Baldwin et al. (1991) or Rubin et al. (1991a,b) were used, one would get a total abundance ratio of about 1/30 of the solar value. This result is between 1.2 and 3.3 times higher than the values derived by Rubin et al. (1997), if one assumes a $N(O)/N(H)$ ratio for Orion of about 1/2 solar. Nevertheless, the present gaseous iron abundance from the Fe $^{3+}$ lines is about a factor of ten lower than our results from Fe $^+$ and Fe $^{2+}$. This large discrepancy exceeds the combined uncertainties of the observations and the atomic data and remains unexplained. A summary of the ionic and total Fe/O abundance ratios estimated for different ionization zones in Orion is presented in Table 8.

8. Summary and Conclusions

The present study of the ionization structure and spectra of Fe I-IV in Orion yields several conclusions that might be generally applicable to low-ionization gaseous nebulae.

The physical processes of spectral formation and photoionization are described in the light of new atomic data for Fe I–IV (Table 1) that should be sufficiently accurate for reliable spectroscopic analysis and modeling of these ions in astrophysical plasmas, although more work is still needed to improve the forbidden transition probabilities (in progress).

The study of forbidden optical emission spectra of [Fe II], under nebular conditions including the effects of collisional excitation, fluorescent excitation by UV continuum, and line self-absorption, reveals fluorescence as relatively inefficient and optical depth effects to be generally negligible. The [Fe II] emission from H II regions like Orion originates largely in high density partially ionized zones (PIZ’s) within the ionization front. This conclusion is derived from numerous line ratio density diagnostics, some of which are insensitive to fluorescent excitation. These line ratios should also be useful for diagnostics of plasmas even when the radiation field is sufficiently intense to affect some of the [Fe II] lines. Moreover, under fluorescent excitation the optical [Fe II] emission should be accompanied by observable dipole allowed Fe II lines that are absent in H II regions like Orion, but are observed in circumstellar nebulae and the subclass of bipolar planetary nebulae with symbiotic star cores (a more detailed study is in progress).

Unlike the optical emission, the [Fe II] near-IR and IR lines can be easily excited at low N_e , while they are collisionally de-excited at the high densities in the PIZ. These lines should therefore originate from a region that extends within the lower density FIZ. Observational studies of the relative intensities of the near-IR [Fe II] lines and their expansion velocities are proposed.

The [Fe III] emission lines are primarily collisionally excited, and the observed line ratios are consistent with the conditions (T_e and N_e) of the FIZ. As expected from the modeled ionization structure of nebulae, there is a correlation between the observed [Fe III] emission and the emission from low ionization species like N^+ and O^+ .

The theoretical [Fe IV] emission spectrum was studied in detail. Under nebular conditions most of the emission lies in the UV, as recently observed (Rubin et al. 1997), while the optical emission is formed only by rather highly excited levels that are difficult to populate. Optical [Fe IV] lines have been identified in only a handful of objects including the bipolar nebula M2-9 (Torres-Peimbert & Arrieta 1996). The presence of these lines indicates unusual conditions for typical nebulae, with high electron densities up to 10^7 cm^{-3} and a high degree of ionization of the plasma.

The observed kinematics of the Orion nebula seem to be well correlated with the physical conditions. There is a distinction in the observed expansion velocities for different species and their degree of ionization. In particular, neutrals and ionized species of low ionization potential, like O^0 , Fe^+ , and Ni^+ , which are expected to emit predominantly from the neutral and partially ionized zones, are distinctly separated by more than 10 km s^{-1} from the fully ionized gas. Moreover, the expansion velocities of optical emission from O^0 , Fe^+ , and Ni^+ are remarkably similar to those of the PDR and the molecular core. This also provides strong evidence for the high densities in the PIZ. Similar kinematic analysis of other H II regions is proposed.

Photoionization modeling of Fe emission in Orion with the new atomic data indicates that the main source of uncertainty is the assumed structure, for example the assumption of static conditions and an *ad hoc* density profile. Particularly problematic is the region near and within the ionization front where neutrals and ions with low first ionization potentials emit, as illustrated by modeling all ionization stages of oxygen (O I–III) in Orion simultaneously. It is found that high densities are required at the I-front to reproduce the observed [OI] emission, but more realistic models would require radiative-hydrodynamic modeling. Also, the roles of enhanced electron and proton impact destruction of grains, particularly in the high density PIZ, and the precise role of charge exchange processes,

remain to be explored.

Finally, the relative gas phase abundance of Fe/O in Orion is determined spectroscopically from [Fe II], [Fe III], and [Fe IV] emission separately. Ionic fractions of Fe and O ions that co-exist are employed and the physical conditions (T_e , N_e) in each emitting region are estimated individually. This approach should be accurate and takes into account temperature and density variations across the nebula. The Fe/O in the PIZ is found to lie between near-solar values down to a conservative lower limit of 1/4 solar. Taking into account the uncertainties, this is generally consistent with our previous determinations in BP95a and BPP96. The Fe/O derived from [Fe III] is about $1/(4 \pm 1)$. For O/H in Orion of about half the solar value, this result agrees with most previous determinations of Fe/H, about one tenth solar (e.g. OTV). In contrast, the Fe/O ratio obtained from [Fe IV] is about 26 times lower than solar. Although considerably higher than the values derived by Rubin et al. (1997), it is still much lower than the determinations from other iron ions. This apparently differential iron gas phase abundance across Orion obtained from different ions is puzzling. It seems unlikely that the emissivities for the [Fe IV] UV lines could be overestimated by as much as a factor of 6, unless the Garstang A-values are in substantial error (work is in progress to check these). However, for conditions in Orion, all of the emission from Fe IV depends mostly on the collision strengths and only marginally on the A-values (in the low N_e limit). It is noted that the 4P and 4D terms that give rise to the strongest [Fe IV] UV lines are populated predominantly via collisional excitation from the first excited state 4G which is highly metastable. Thus, one may expect that the emissivity of the observed lines would be very sensitive to radiative de-population of the 4G state to the ground state, yet we observe that an increase of the ($^4G_J - ^6S_{5/2}$) A-values of *three orders of magnitude* reduces the emissivity of the 2836.6 Å line by less than a factor of two. On the other hand, the new collision strengths should be quite accurate, as discussed in Sections 2 and 3.5. Another possibility would be that

the ionic fractions for the iron ions are in error. If the iron abundances from Fe^{2+} and Fe^{3+} were to be reconciled in this way the $X(\text{Fe}^{3+})/X(\text{Fe}^{2+})$ ionic ratio would be about 0.27 instead of the value of 1.8 expected from our present model, 3.4 from Baldwin et al. (1991), and 1.3 from Rubin et al. (1991b); the actual gas phase Fe/O would then be about 1/14, or $\text{Fe}/\text{H} \sim 1/28$, of the solar ratios. But such a low ratio for the ionic fractions would require a combined error from the photoionization cross sections and recombination coefficients of nearly an order of magnitude. This appears rather unlikely, especially since the unified recombination coefficients in the present work are calculated using the same *ab initio* close-coupling method as the photoionization data, ensuring self-consistency and minimizing the possibility of any large errors in relative ionic fractions. Alternatively, if the stellar radiation field were adjusted to reproduce this low ionic ratio, the ionic fractions for all other elements, e.g. C, N, O, S, etc., would also be affected. It is rather difficult to reconcile the abundances derived from each ion, suggesting a gradient in the gas phase iron abundance in Orion via some unknown mechanism.

We would like to thank Mike Barlow, Xiao-wei Liu, Don Osterbrock, and Manuel Peimbert for discussions and suggestions. We are also grateful to Mónica Rodríguez for providing us with her observations of [FeII] and [FeIII] data. This work was supported in part by grants from the U.S. National Science Foundation for the Iron Project (PHY-9421898), and the NASA Long Term Space Astrophysics program (NAS5-32643). The computational work was carried out on the Cray Y-MP and the massively parallel Cray T3D at the Ohio Supercomputer Center in Columbus Ohio.

REFERENCES

- Aller, L.H. 1987, In: Spectroscopy of Astrophysical Plasmas, ed. A. Dalgarno & D. Layzer (Cambridge: Cambridge Univer. Press), 89.
- Baldwin, J.A., et al. 1996, ApJ, 468, L115 (B96).
- Baldwin, J.A., Ferland, G.J., Martin, P.G., Corbin, M.R., Cota, S.A., Peterson, B.M., Slettebak, A. 1991, ApJ, 374, 580.
- Balick, B., 1989, AJ, 97, 476.
- Balick, B., Gammon, R.H., & Hjellming, R.M. 1974, PASP, 86, 616.
- Bautista, M.A. 1997, A&AS, 122, 167.
- 1996, A&AS, 119, 105.
- Bautista, M.A., Peng, J., & Pradhan, A. K. 1996, ApJ, 460, 372 (BPP).
- Bautista, M. A., Pogge, R. W., & DePoy, D. L. 1995, ApJ, 452, 685.
- Bautista, M.A., & Pradhan, A.K. 1997. A&AS, (in press).
- 1996, A&AS, 115, 551 (BP96).
- 1995a, ApJ, 442, L65 (BP95a).
- 1995b, J. Phys. B: At. Opt. Phys., 28 L173.
- Bautista, M.A., Pradhan, A.K., & Osterbrock, D.E. 1994, ApJ, 432, L135.
- Bedijn, P.J. & Tenorio-Tagle, G. 1981, A&AS, 98, 85.
- Berrington, K. A. & Pelan, J.C. 1995, A&AS, 114, 367.
- Berrington, K. A. & Pelan, J.C. 1997, Erratum, A&AS (in press).
- Berrington K. A., Zeippen, C. J., Le Dourneuf M., Eissner W., & Burke P. G. 1991, J. Phys B: At. Mol. Opt. Phys., 24, 3467.

- Bodenheimer, P., Tenorio-Tagle, G., & Yorke, H.W. 1979, *ApJ*, 233, 85.
- Böhm, K.H. & Solf, J. 1990, *ApJ*, 348, 297.
- Castañeda, H.O. 1988, *ApJS*, 67, 93.
- Conti, P.S. & Alshuler, W.R. 1971, *ApJ*, 170, 325.
- Corradi, R.L.M. 1995, *MNRAS*, 276, 521.
- Cowan R.D., 1981, *The theory of Atomic Structure and Spectra*, University of California Press, Berkeley, California.
- Dennefeld, M. 1982, *A&A*, 112, 215.
- 1986, *A&A*, 157, 267.
- Dennefeld, M. & Péquignot, D. 1983, *A&A*, 127, 42.
- DePoy, D.L. & Pogge, R.W. 1994, *ApJ*, 433, 725.
- Eissner W, Jones M and Nussbaumer H 1974, *Comput. Phys. Commun.* 8, 270
- Fehrenbach, Ch. 1977, *A&A*, 29, 71.
- Ferland, G.J. 1993, University of Kentucky Department of Physics and Astronomy Internal Report (CLOUDY).
- García-Segura, G. & Franco, J. 1996, *ApJ*, 469, 171.
- Garstang, R.H. 1957, *MNRAS*, 117, 393
- 1958, *ApJ*, 6, 572.
- 1962, *MNRAS*, 124, 321.
- Giridhar, S. & Ferro, A.A. 1995, *Rev. Mexicana de Astronomía y Astrofis.*, 31, 23.
- Goudis, C. 1982, *The Orion Complex: A Case Study of Interstellar Matter* (Dordrecht: Reidel).

- Grandi, S.A. 1975, ApJ, 199, L43.
- Greve, A., Castles, J., & McKeith, C.D. 1994, A&A, 284, 919.
- Hamann, F. & DePoy, D.L. 1994, 422, 626.
- Henry, R. B. C., MacAlpine, G. M., & Kirshner, R. P. 1984, ApJ, 278, 619.
- Hudgins D., Herter T., & Joyce R. J. 1990, ApJ, 354, L57.
- Hummer, D.G., Berrington, K. A., Eissner, W., Pradhan, A. K., Saraph, H. E., & Tully, J. A. 1993, A&A, 279, 298.
- Johnson, D. R. H., Barlow, M. J., Drew, J. E., & Brinks, E. 1992, MNRAS, 255, 261.
- Kaler, J.B. 1967, ApJ, 148, 925.
- Kaler, J.B., Aller, L.H., & Bowen, I.S. 1965, ApJ, 141, 912.
- Kelly H.P. 1972, Phys Rev A 6, 1048.
- Kurucz, R.L., 1979, ApJS, 40, 1.
- Le Dourneuf M., Nahar, S.N., & Pradhan, A.K. 1993, J. Phys. B: At. Opt. Phys., 26, L1.
- Lowe, R.P., Moorhead, J.M., & Wehlau, W.H. 1979, ApJ, 228, 191.
- Lucy L.B. 1995, A&A, 294, 555.
- Mihalas, D. 1978, *Stellar Atmospheres*, 2nd Edition, (W. H. Freeman and Company).
- Nahar, S.N. 1995, A&A 293, 967.
- 1996a, Phys. Rev. A, 53, 1545.
- 1996b, Phys. Rev. A, 53, 2417.
- 1997, Phys. Rev. A, 55, 1980.
- Nahar, S. N., Bautista, M.A., & Pradhan, A.K. 1997, ApJ, 479, 497.
- Nahar, S.N., and Pradhan, A.K. 1992, Phys. Rev. Lett., 68, 1488.

- 1994a, Phys. Rev. A, 49, 1816.
- 1994b, J. Phys. B: At. Opt. Phys., 27, 429.
- 1996, A&AS, 119, 509.
- Neufeld, D. A. & Dalgarno, A. 1987, Phys. Rev. A, 35, 3142.
- Nussbaumer, H., & Storey, P. J. 1988, A&A, 193, 327.
- O’Dell, C.R. & Wen, Z. 1992, ApJ, 387, 229.
- O’Dell, C.R., Wen, Z., & Hester, J.J. 1991, PASP, 103, 824.
- Osterbrock, D. E. 1989, *Astrophysics of Gaseous Nebula and Active Galactic Nuclei* (Mill Valley: University Science Books).
- Osterbrock, D. E., Shaw, R. A., & Veilleux, S. 1990, ApJ, 352, 561.
- Osterbrock, D.E., Tran, H.D., & Veilleux, S. 1992, ApJ, 389, 305. (OTV)
- Peimbert, M., 1967, ApJ, 150, 825.
- Peimbert, M., 1995, in: *The Analysis of Emission Lines*, ed. R.E. Williams, Cambridge University Press.
- Peimbert, M., Esteban, C., Torres-Peimbert, S., & Escalante, V. 1996, BAAS, 28, 1333.
- Pogge, R.W., Owen, J.M., & Atwood, B. 1992, ApJ, 399, 147.
- Pradhan, A. K. & Zhang, H. L. 1993, ApJ, 409, L77.
- Quinet, P., Le Dourneuf, M., and Zeippen, C.J., 1997, A&AS, (in press).
- Reilman, R.F. & Manson, S.T. 1979, ApJS, 40, 815 (RM).
- Riera, A., Garcia-Lario, P., Manchado, A., Pottasch, A.R., & Raga, A.C. 1995, A&A, 302, 137.
- Rodríguez, M. 1996, A&A, 313, L5.

- Rubin, R. H., et al. 1997, ApJ, 474, L131.
- Rubin, R.H., Simpson, J.P., Haas, M.R., & Erickson, E.F. 1991a, 374, 564.
- , 1991b, PASP, 103, 834.
- Rudy, R. J., Rossano, G. S., & Puetter, R. C. 1994, ApJ, 426, 646.
- Seaton, M.J., Yu Yan, Mihalas, D., & Pradhan, A.K. 1994, MNRAS, 266, 805.
- Sawey, P.M., & Berrington, K.A. 1992, J. Phys. B: At. Opt. Phys., 25, 1451.
- Sellmaier, F.H., Yamamoto, T., Pauldrach, A.W.A., Rubin, R.H. 1996, A&A, 305, L37.
- Stahl O. & Wolf B., 1986, A&A, 158, 371.
- Sugar J. and Corliss C. 1985, J. Phys. Chem. Ref. Data, 14, Suppl. 2.
- Tenorio-Tagle, G. 1977, A&A, 61, 189.
- Tielens, A.G.G.M. & Hollenbach, D. 1985, ApJ, 291, 747.
- Torres-Peimbert. S. & Arrieta, A. 1996, BASS, 189, 9711.
- Verner, D. A., Yakovlev, D. G., Brand, I. M., Trzhaskovskaya, M. B. 1993, At. Data Nucl. Data Tab. 55, 233.
- Wen, Z. & O’Dell, C.R. 1995, ApJ, 438, 784.
- Woods, D.T., Shull, J.M., and Sarazin, C.L. 1981, ApJ, 249, 399.
- Zhang H.L. 1996, A&AS, 119, 523.
- Zhang, H.L., & Pradhan, A.K., 1995a, A&A, 293, 953 (ZP95).
- 1995b, J. Phys. B: At. Opt. Phys. 28, 3403.
- 1997, *Astronomy and Astrophys. Supplement Series*, (*in press*).

Table 1. New Atomic Data For Fe I–V : (Iron Project Calculations at Ohio State)

Ion	Photoionization	Recombination	Collis. Excitation	Transition Prob.
Fe I	1	2	–	3
Fe II	4	5	6	7
Fe III	8	9	10	11
Fe IV	12	13	14	15
Fe V	16	17	–	18

1. σ_{PI} for 563 bound states multiplets (Bautista & Pradhan 1995b; Bautista 1997); **2.** $\alpha_R(T)$ - recombination rate coefficients (Nahar et al. 1997); **3.** A-coefficients and gf-values for 27,000 LS multiplets (Bautista 1997); **4.** σ_{PI} for 745 bound states (Le Dourneuf et al. 1993; Nahar & Pradhan 1994b); **5.** $\alpha_R(T)$ - Nahar (1997); **6.** $\Upsilon(T)$ - for 12,561 fine structure transitions among 142 levels (Zhang & Pradhan 1995a); **7.** A-coefficients and gf-values for dipole transitions among 19,267 LS multiplets and 234,689 fine structure transitions (Nahar 1995); **8.** σ_{PI} for 805 bound states (Nahar 1996a); **9.** $\alpha_R(T)$ (Nahar 1996b); **10.** $\Upsilon(T)$ for 23,871 transitions among 219 fine structure levels (Zhang 1996); **11.** A-coefficients and gf-values for allowed transitions among 1408 LS multiplets and 9797 fine structure transitions; A-coefficients for 362 forbidden fine structure transitions (Nahar & Pradhan 1996); **12.** σ_{PI} for 746 bound states (Bautista & Pradhan 1997); **13.** $\alpha_R(T)$ (Nahar, Bautista, & Pradhan; to be submitted); **14.** $\Upsilon(T)$ for 8,771 transitions among 140 levels (Zhang & Pradhan 1997); **15.** A-coefficients and gf-values for dipole transitions among 34,635 LS multiplets (Bautista and Pradhan 1997); **16.** σ_{PI} for 1812 bound states (Bautista 1996); **17.** $\alpha_R(T)$, (Nahar, Bautista & Pradhan; to be submitted); **18.** A-coefficients and gf-values for 129,904 LS multiplets (Bautista 1996).

Table 2. Comparison of $\Upsilon(T = 10^4\text{K})$ values for Fe II

Transition	Present(23CC)	BP96(18CC)	ZP95(38CC)
${}^6D_{9/2}$			
– ${}^6D_{7/2}$	5.260	4.65	5.52
– ${}^6D_{5/2}$	1.300	1.29	1.49
– ${}^6D_{3/2}$	0.641	0.813	0.675
– ${}^6D_{1/2}$	0.297	0.433	0.284
– ${}^4F_{9/2}$	1.49	1.31	3.60
– ${}^4F_{7/2}$	0.566	0.614	1.51
– ${}^4F_{5/2}$	0.120	0.135	0.497
– ${}^4D_{7/2}$	8.040	14.30	10.98
– ${}^4D_{5/2}$	0.445	0.572	0.560
– ${}^4D_{3/2}$	0.167	0.386	0.191
– ${}^4P_{5/2}$	0.722	0.542	0.948
– ${}^4P_{3/2}$	0.404	0.319	0.502
– $b {}^4P_{5/2}$	0.273	0.215	0.308
– ${}^4H_{13/2}$	0.543	0.196	0.631
– ${}^4H_{11/2}$	0.256	0.196	0.311
– $b {}^4H_{9/2}$	0.420	0.081	0.402
– $b {}^4F_{7/2}$	0.188	0.039	0.216
– ${}^6S_{5/2}$	0.857	0.399	—
– ${}^4G_{11/2}$	0.435	0.373	0.344
– ${}^4G_{9/2}$	0.186	0.180	0.215

Table 3. Comparison of ratios of A-values for near-IR lines with observations

Line ratio				
Transitions	Wavelength(μm)	Observed ^a	N & S ^b	QLZ ^c
$\frac{a^4 D_{7/2} - a^6 D_{9/2}}{a^4 D_{7/2} - a^4 F_{9/2}}$	$\frac{1.257}{1.644}$	1.34	1.36	1.04
$\frac{a^4 D_{7/2} - a^6 D_{7/2}}{a^4 D_{7/2} - a^4 F_{9/2}}$	$\frac{1.298}{1.644}$	0.38	0.36	0.23
$\frac{a^4 D_{7/2} - a^4 F_{7/2}}{a^4 D_{7/2} - a^4 F_{9/2}}$	$\frac{1.677}{1.644}$	0.13	0.20	0.41
$\frac{a^4 D_{5/2} - a^4 F_{9/2}}{a^4 D_{5/2} - a^6 D_{5/2}}$	$\frac{1.534}{1.295}$	0.84	1.06	1.33
$\frac{a^4 D_{5/2} - a^6 D_{3/2}}{a^4 D_{5/2} - a^6 D_{5/2}}$	$\frac{1.328}{1.295}$	0.54	0.61	0.58
$\frac{a^4 D_{5/2} - a^4 F_{7/2}}{a^4 D_{5/2} - a^6 D_{5/2}}$	$\frac{1.677}{1.295}$	0.80	0.77	0.97
$\frac{a^4 D_{3/2} - a^6 D_{3/2}}{a^4 D_{3/2} - a^4 F_{7/2}}$	$\frac{1.279}{1.599}$	0.72	0.86	0.73
$\frac{a^4 D_{3/2} - a^6 D_{1/2}}{a^4 D_{3/2} - a^4 F_{7/2}}$	$\frac{1.298}{1.599}$	0.51	0.38	0.32
$\frac{a^4 D_{3/2} - a^4 F_{5/2}}{a^4 D_{3/2} - a^4 F_{7/2}}$	$\frac{1.712}{1.599}$	0.25	0.26	0.26
$\frac{a^4 D_{1/2} - a^4 F_{5/2}}{a^4 D_{1/2} - a^6 D_{1/2}}$	$\frac{1.644}{1.271}$	0.64	0.98	1.38

^aNear-IR spectra of HH1 by Everett & Bautista (1996; unpublished)

^bNussbaumer & Storey (1988)

^cQuinet et al. (1997)

Table 4. Comparison of ratios of A-values for optical lines with observations

Line ratio				
Transitions	Wavelength (Å)	Observed ^a	G62 ^b	QLZ ^c
$a \ ^4G_{7/2} - a \ ^4F_{3/2}$	<u>4372.4</u>			
$a \ ^4G_{7/2} - a \ ^4F_{5/2}$	<u>4319.6</u>	0.83	0.52	0.51
$a \ ^4G_{9/2} - a \ ^4F_{7/2}$	<u>4296.9</u>	1.70	2.13	2.21
$a \ ^4G_{9/2} - a \ ^4F_{5/2}$	<u>4352.8</u>			
$a \ ^4G_{9/2} - a \ ^4F_{7/2}$	<u>4276.8</u>	2.12	4.53	3.98
$a \ ^4G_{9/2} - a \ ^4F_{9/2}$	<u>4177.2</u>			
$a \ ^4G_{9/2} - a \ ^4F_{5/2}$	<u>4352.8</u>	1.24	2.12	1.80
$a \ ^4G_{9/2} - a \ ^4F_{9/2}$	<u>4177.2</u>			
$b \ ^4F_{5/2} - a \ ^4F_{7/2}$	<u>4874.5</u>	1.17	1.04	1.35
$b \ ^4F_{5/2} - a \ ^6D_{5/2}$	<u>4488.8</u>			
$b \ ^4F_{5/2} - a \ ^4F_{5/2}$	<u>4973.4</u>	0.50	0.84	1.08
$b \ ^4F_{5/2} - a \ ^6D_{5/2}$	<u>4488.8</u>			
$b \ ^4F_{5/2} - a \ ^4F_{3/2}$	<u>5073.4</u>	0.50	0.39	0.56
$b \ ^4F_{5/2} - a \ ^6D_{5/2}$	<u>4488.8</u>			
$b \ ^4F_{9/2} - a \ ^4F_{9/2}$	<u>4814.6</u>	5.50	6.22	7.60
$b \ ^4F_{9/2} - a \ ^6D_{5/2}$	<u>4492.6</u>			
$a \ ^4H_{9/2} - a \ ^4F_{7/2}$	<u>5220.1</u>	3.40	4.86	5.15
$a \ ^4H_{9/2} - a \ ^4F_{9/2}$	<u>5072.4</u>			
$a \ ^4H_{9/2} - a \ ^4F_{5/2}$	<u>5333.7</u>	9.40	11.2	12.4
$a \ ^4H_{9/2} - a \ ^4F_{9/2}$	<u>5072.4</u>			
$b \ ^4P_{5/2} - a \ ^6D_{7/2}$	<u>4889.6</u>	3.20	3.69	2.51
$b \ ^4P_{5/2} - a \ ^4F_{7/2}$	<u>5432.2</u>			
$b \ ^4P_{3/2} - a \ ^6D_{3/2}$	<u>4774.7</u>	0.072	0.094	0.065
$b \ ^4P_{3/2} - a \ ^4F_{7/2}$	<u>5158.8</u>			
$a \ ^4H_{11/2} - a \ ^4F_{7/2}$	<u>5261.6</u>	2.70	3.01	3.24
$a \ ^4H_{11/2} - a \ ^4F_{9/2}$	<u>5111.6</u>			
$a \ ^4P_{5/2} - a \ ^4F_{7/2}$	<u>9051.9</u>	0.21	0.23	0.24
$a \ ^4P_{5/2} - a \ ^4F_{9/2}$	<u>8617.0</u>			
$a \ ^4P_{3/2} - a \ ^4F_{3/2}$	<u>9470.9</u>	0.13	0.15	0.16
$a \ ^4P_{3/2} - a \ ^4F_{7/2}$	<u>8891.9</u>			
$a \ ^4P_{1/2} - a \ ^4F_{3/2}$	<u>9267.5</u>	1.40	1.26	1.29
$a \ ^4P_{1/2} - a \ ^4F_{5/2}$	<u>9033.5</u>			

^aOptical spectra of HH1 Böhm & Solf (1990)

^bGarstang (1962)

^cQuinet et al. (1997)

Table 5. Relative intensity of [Fe II] lines in Orion

λ (Å)	Observed		Present ^e			B96	
	I/I(8617) ^a	(I)[PIZ%] ^f	(II)[PIZ%] ^f	(III)	(A)	(B)	(C)
8892	0.19	0.31[32%]	0.33[33%]	0.27	0.31	0.31	0.36
7452	0.51	0.22[60%]	0.26[61%]	0.12	—	—	—
7155	1.47	0.73[60%]	0.84[61%]	0.39	—	—	—
5159 ^b	1.3	2.3[37%]	1.4[69%]	1.8	1.7	1.9	1.1
5262	0.81	0.90[47%]	0.64[77%]	0.61	0.28	0.31	0.26
5334	0.33	0.43[69%]	0.40[87%]	0.18	0.22	0.24	0.21
4815 ^b	0.94	0.61[48%]	0.48[72%]	0.41	1.1	1.2	0.71
4245	0.87	2.0[23%]	0.69[79%]	2.0	2.1	2.4	1.3
4277 ^c	0.64	0.52[46%]	0.34[84%]	0.36	0.46	0.50	0.37
4287	1.29	0.31[67%]	0.31[79%]	0.13	—	—	—
12567 ^d	3.3-4.2	3.2[04%]	3.4[04%]	4.1	3.5	3.4	2.6
	σ	0.65	0.40	0.63	0.69	0.80	0.53

^aLine intensities corrected for extinction from OTV except for the 12567 Å line.

^bUnresolved [FeII] blends.

^cPossibly blended with OII λ 4275.6 and 4276.8 Å

^dMeasurements from Lowe et al. (1979; lower value) and Bautista et al. (1995; higher value).

^e(I) PIZ and FIZ with fluorescence; (II) PIZ and FIZ without fluorescence; (III) only FIZ with fluorescence.

^fThe percentage contribution of the PIZ to the total intensity of the line is indicated brackets. The contributions of the PIZ to the 8617 Å line are 24% in model (I) and 28% in (II).

Table 6. Optical spectrum of oxygen in Orion vs. photoionization models

Ion	line (Å)	Observed/I(H β) \times 100			B96			Present ^b				
		OTV	B96	G94 ^a	(A)	(B)	(C)	(I)	(II)	(III)	(IV)	(V)
[O I]	6300	0.959	0.722	0.70	0.341	0.336	0.699	0.34	0.20	0.17	0.75	0.91
[O I]	5577	0.058	< 0.0136	—	0.0044	0.0043	0.0095	0.004	0.002	0.002	0.006	0.009
[O II]	3727	146	94	123	188	188	149	186	209	145	126	132
	7320	6.21	—	7.10	—	—	—	13.8	7.86	4.44	11.6	9.19
	7330	5.47	—	5.92	—	—	—	11.2	6.35	3.56	9.40	7.45
[O III]	4363	1.39	—	1.00	—	—	—	1.93	2.39	0.74	0.69	0.79
	4959	100.2	—	104.8	—	—	—	132	169	87.8	75.9	87.6
	5007	302	343	—	465	460	379	395	507	263	228	263

^aGreve et al. (1994)

^bResults from present photoionization models including the contribution from a high density ionization front (see text for an explanation of the different models)

Table 7. $\text{Fe}^{2+}/\text{O}^+$ abundance ratios in Orion

$\lambda(\text{\AA})$	Transition	$I_{\text{Fe}^{2+}}(\lambda)/I_{\text{O}^+}(3727)$	$N(\text{Fe}^{2+})/N(\text{O}^+)$
5412	$a^5D_1 - a^3P_2$	2.4×10^{-4}	0.0084
5270	$a^5D_3 - a^3P_2$	3.7×10^{-3}	0.012
4987	$a^5D_4 - a^3H_6$	2.3×10^{-4}	0.003
	$+a^5D_3 - a^3H_4$		
4881	$a^5D_4 - a^3H_4$	2.9×10^{-3}	0.0092
4658	$a^5D_4 - a^3F_4$	9.2×10^{-3}	0.036
4702	$a^5D_3 - a^3F_3$	1.7×10^{-3}	0.0099
4734	$a^5D_2 - a^3F_2$	5.6×10^{-4}	0.0095
4607	$a^5D_4 - a^3F_3$	4.2×10^{-4}	0.013
4755	$a^5D_3 - a^3F_4$	1.2×10^{-3}	0.012
4769	$a^5D_2 - a^3F_3$	6.3×10^{-4}	0.011
4778	$a^5D_1 - a^3F_2$	4.5×10^{-4}	0.016

Table 8. Fe/O abundance ratios in Orion

Zone	$\text{Fe}^{i+}/\text{O}^{j+}$	Fe/O	$(\text{Fe}/\text{O})/(\text{Fe}/\text{O})_{\odot}$
$Fe^+ - O^0$	0.065	0.010 - 0.065	1/4 - 3/2
$Fe^{2+} - O^+$	0.014 ± 0.004	0.015 ± 0.005	$1/(3.7 \pm 1.0)$
$Fe^{3+} - O^{2+}$	0.0020 ± 0.0006	0.0017 ± 0.0005	$1/(26 \pm 8)$

Figure Captions

Figure 1. Photoionization cross sections for the ground states of Fe I–V including detailed autoionization resonances. Also plotted are the results of Reilman & Manson (1979; square dots) and Kelly (1972; dashed line).

Figure 2. New recombination rate coefficients for Fe I (Nahar, Bautista, & Pradhan 1997), Fe II (Nahar 1997), and Fe III (Nahar 1996b). These rates are compared with previous dielectronic plus radiative recombination results by Woods et al. (1981; dashed line).

Figure 3. Energy diagram of Fe II with infrared and optical lines considered.

Figure 4. [Fe II] line ratios vs. $\log N_e$ (cm^{-3}) for $T_e = 10000$ K. The different curves represent pure collisional excitation (solid), collisional and fluorescent excitation without optical depth effects (dotted), collisional and fluorescent excitation including line self-shielding (long dashed), and collisional and fluorescent excitation for a UV field ten times that in Orion (short dashed). Collisionally excited line ratios calculated with collision strengths of the present 23CC calculation (short-dash and dot curves) are also shown. The predicted line ratios by Baldwin et al. (1996) are indicated by square dots. The horizontal lines indicate the observed values by OTV (solid) and Rodríguez (1996; dashed lines).

Figure 5. Similar to Fig. 4 but, with optical measurements by OTV and near-IR observations by Lowe et al. (1979; dotted line) and Bautista et al. (1995; solid line).

Figure 6. Energy diagram of Fe III with infrared and optical lines considered.

Figure 7. [Fe III] line ratios vs. $\log N_e$ (cm^{-3}) for $T_e = 9000$ K. The horizontal lines indicate the observed values in Orion by OTV (solid) and the range of values by Greve et al. (1994; dotted lines), and Rodríguez (1996; dashed lines) for optical lines and Bautista et al. (1995; dotted lines) and DePoy & Pogge (1994; dashed lines) for the near-IR lines.

Figure 8. Energy diagram of Fe IV with optical and ultraviolet lines considered.

Figure 9. [Fe IV] line ratios vs. $\log N_e$ (cm^{-3}) for $T_e = 9000$ K.

Figure 10. Line ratio N_e diagnostics from [Fe IV] and [O III] optical lines of high density plasma in the planetary nebula with a symbiotic star core M2-9. Observations by Torres-Peimbert & Arrieta (1996).

Figure 11. [O I] $\lambda\lambda 6300 + 6364$ to $\lambda 5578$ line ratio vs. $\log N_e$ (cm^{-3}) for $T = 5000, 8000, 9000, 10000,$ and 20000 K. The value of this line ratio reported by OTV and the upper limits given by Baldwin et al. (1996; HST and CTIO) are represented by horizontal dashed lines.

Figure 12. The observed velocities of optical lines in Orion vs. the minimum photon energy required to produce the ionized specie (adapted from Kaler 1967 and Balick et al. 1974). The velocities of the molecular cloud (OMC-1) and the photodissociation region (PDR) are also indicated. The observations are from Kaler (1967; empty squares), Fehrenbach (1977; filled circles), and O’Dell & Wen (1992; filled squares).

Figure 13. Computed physical conditions of a constant gas pressure cloud as a function of the distance from the illuminated face.

Figure 14. Sample of ionizing fluxes vs. the photon energy near the illuminated face (a) and near one half thickness of the cloud (b). The ionization limits for Fe I–III are also indicated.

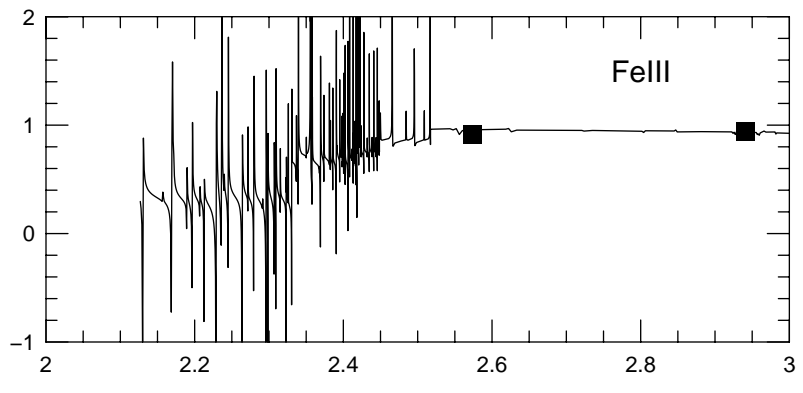
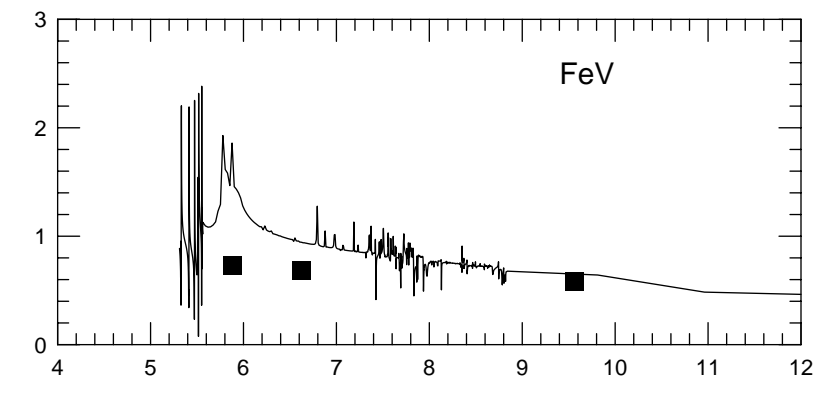
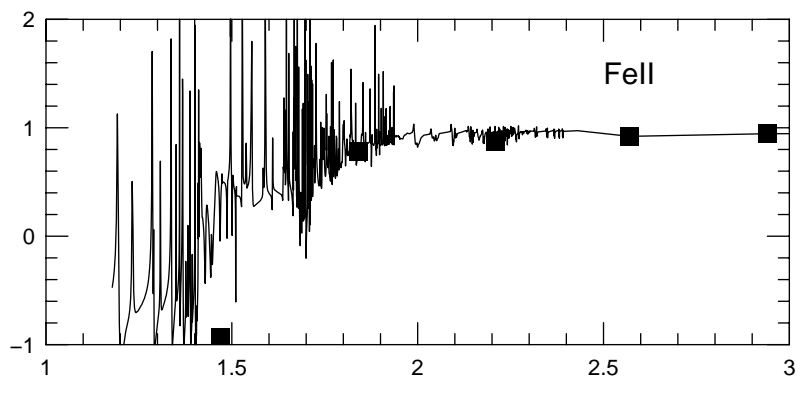
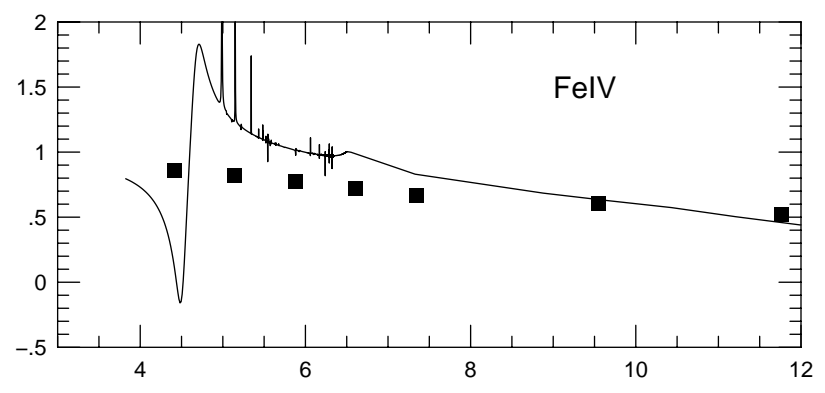
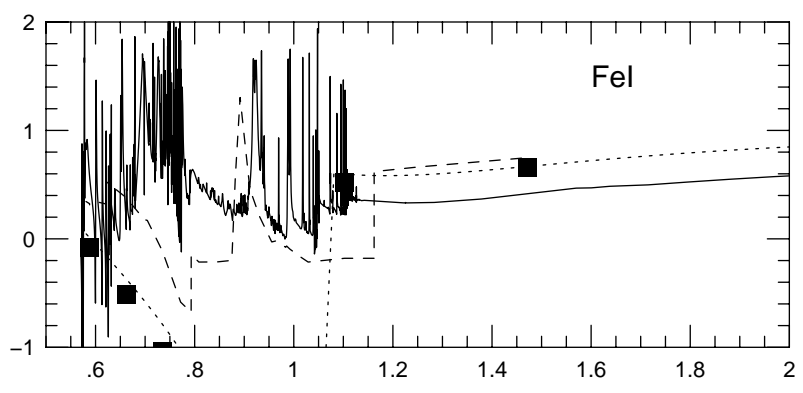
Figure 15. Computed photoionization rates in arbitrary units for Fe I–III as a function of the distance from the illuminated face of the cloud. The solid curves represent the results using the new photoionization cross sections. These are compared with the results obtained with cross sections by Reilman & Manson (1979; dotted curves) and Kelly (1972; dashed curve).

Figure 16. Computed ionization structure of iron in a constant gas pressure cloud as a function of the distance from the illuminated face. The results with the new photoionization-recombination data (solid curves) are compared with the results from CLOUDY (dotted curves).

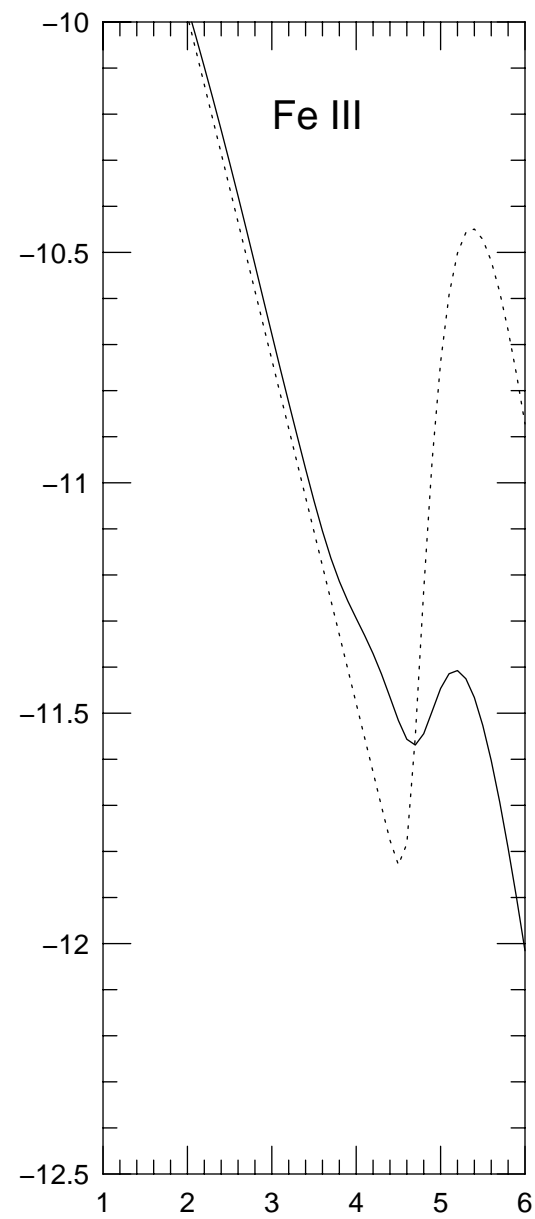
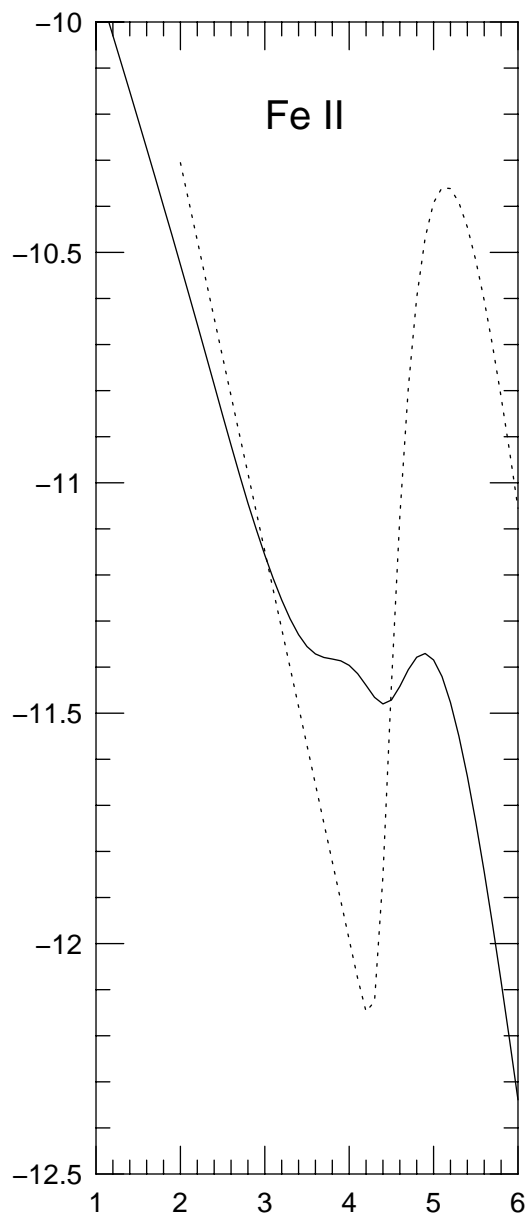
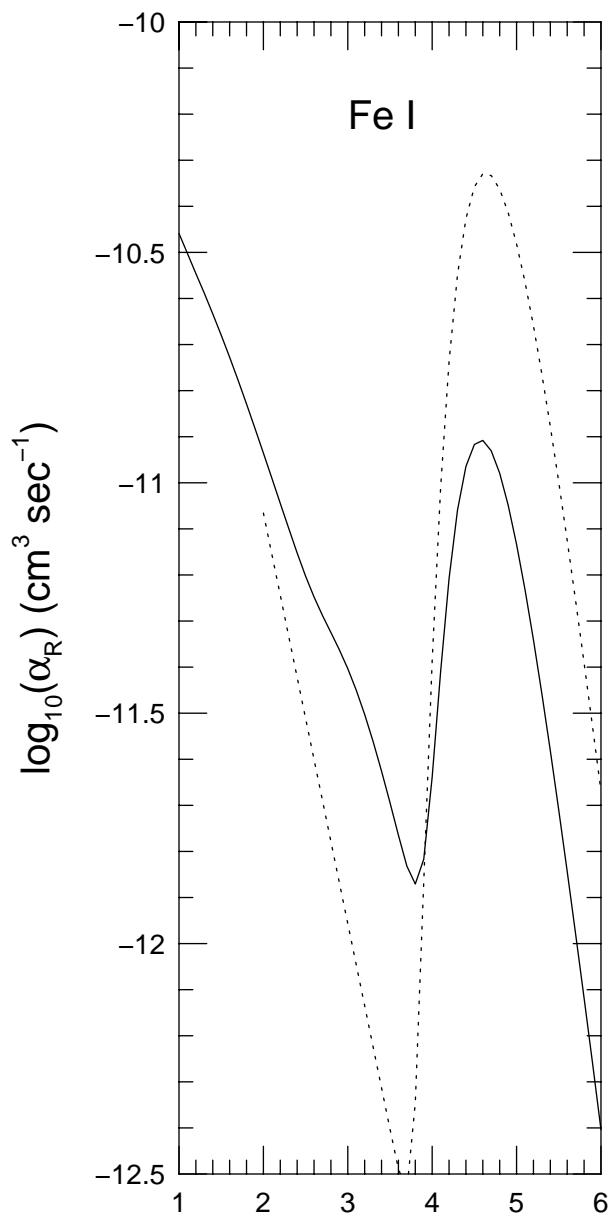
Figure 17. The $\text{Fe}^{2+}/\text{O}^+$ abundance ratio in Orion as a function of the assumed temperature and electron density of the region. The line intensities are from OTV for $I_{\text{Fe}^{2+}}(\lambda 4881)$ and $I_{\text{O}^+}(\lambda 3728)$ (solid curves) and $I_{\text{O}^+}(\lambda 7322)$ (dashed curves).

Figure 18. The $\text{Fe}^{3+}/\text{O}^{2+}$ abundance ratio in Orion as a function of the assumed temperature and electron density of the region. The line intensities are from Rubin et al. (1997) for the [Fe IV] 2827 Å line and from OTV for the [O III] 4363 Å (solid line) and the [O III] 4959 Å line (dashed line).

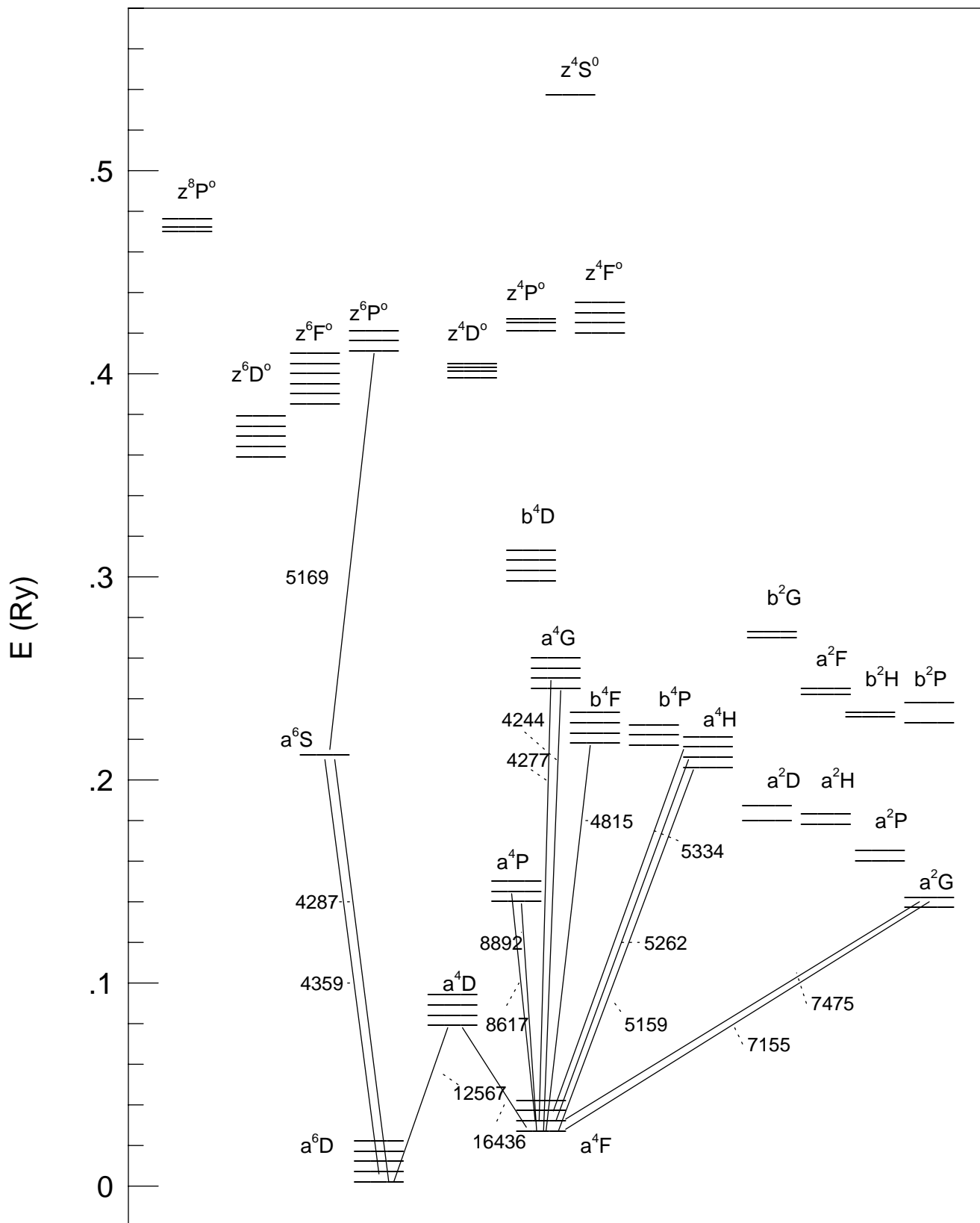
Log₁₀ photoionization cross section [Mb]

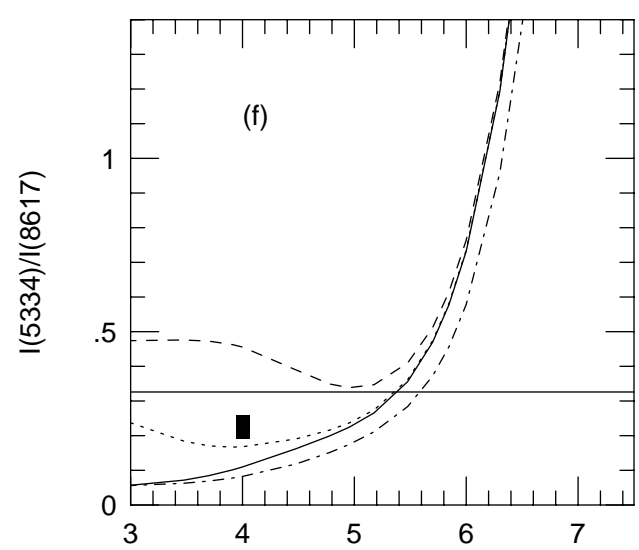
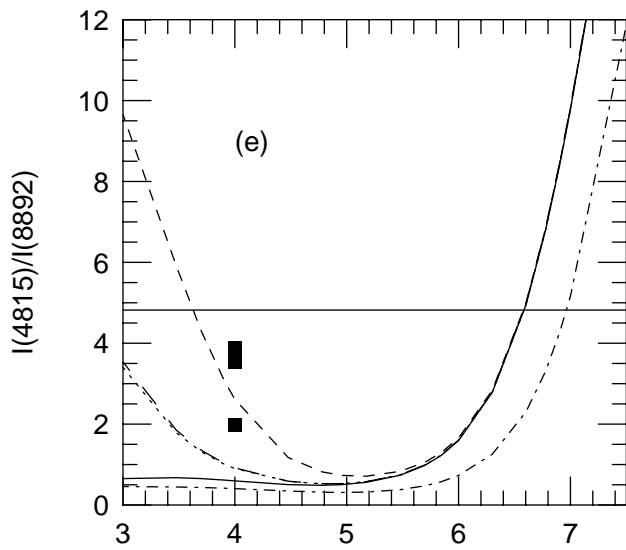
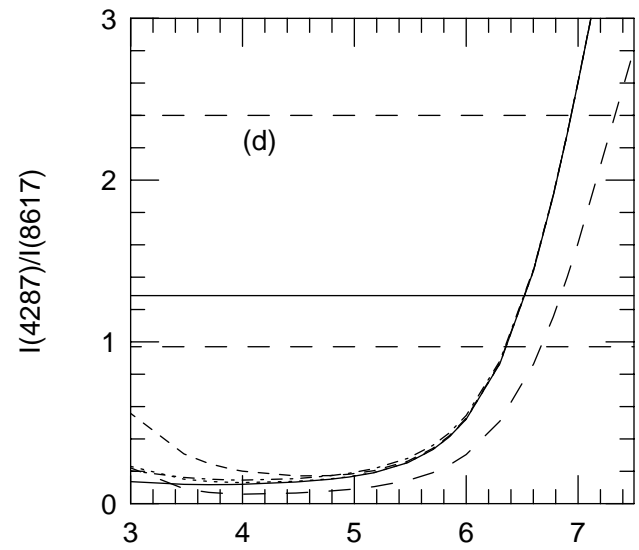
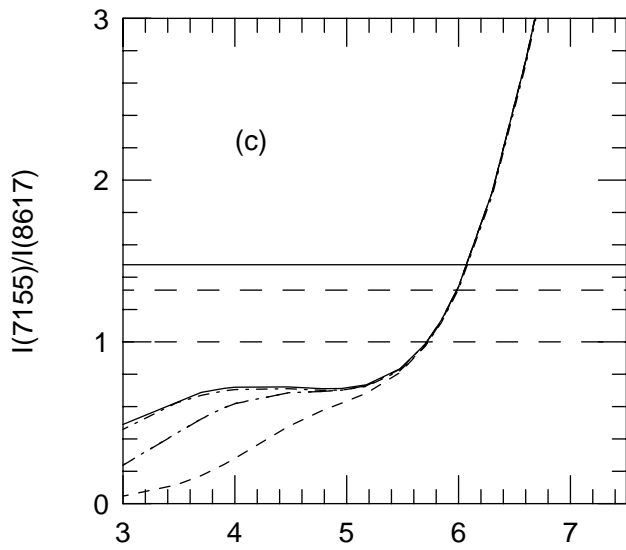
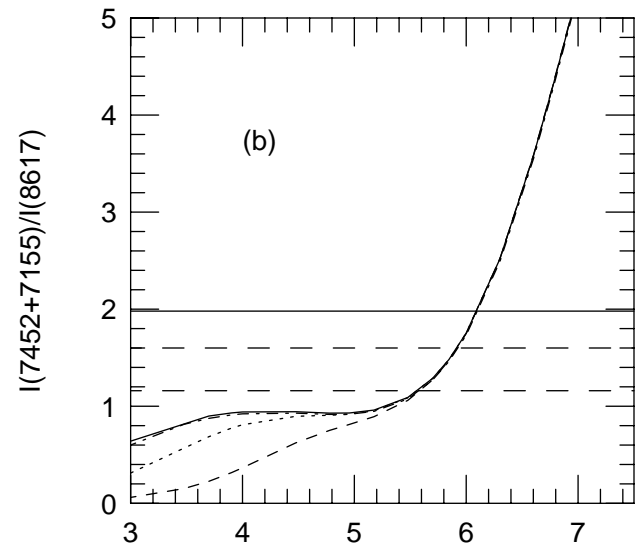
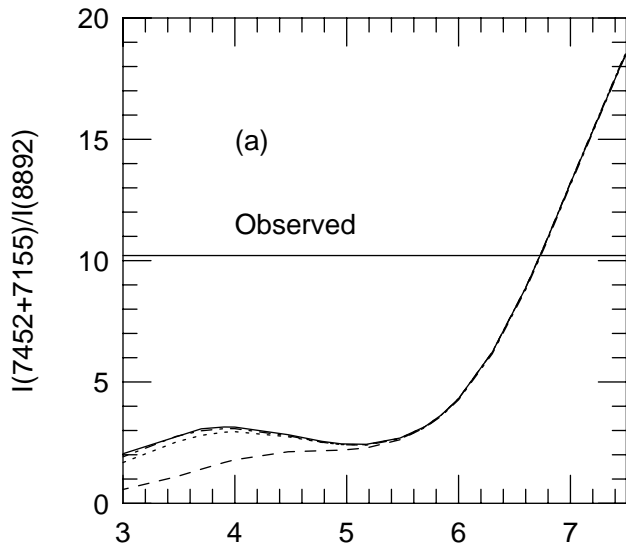


Energy [Ry]

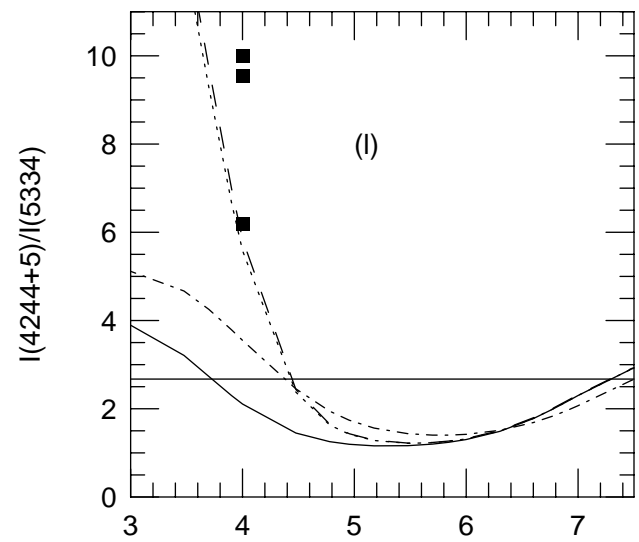
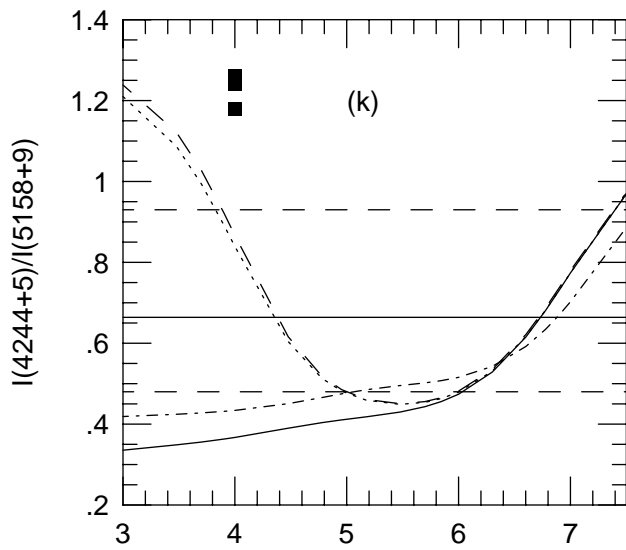
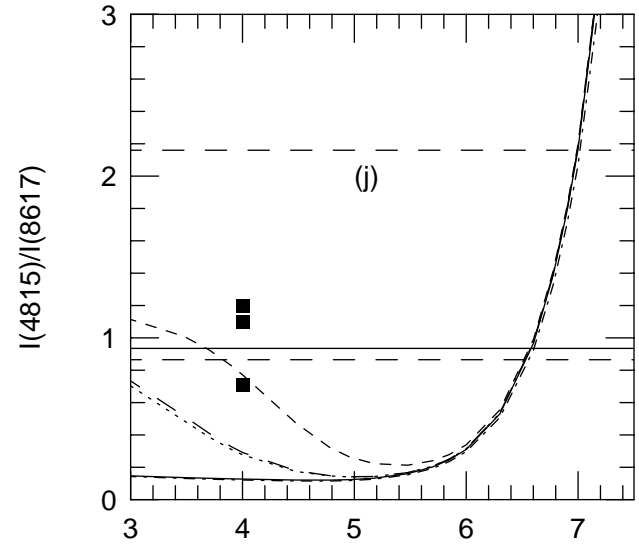
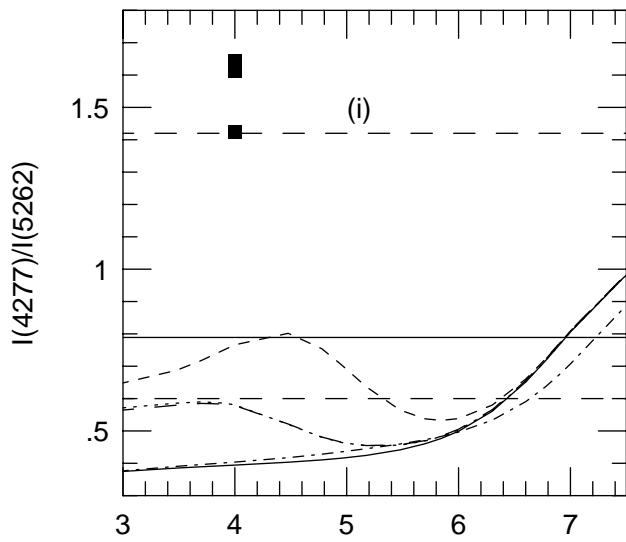
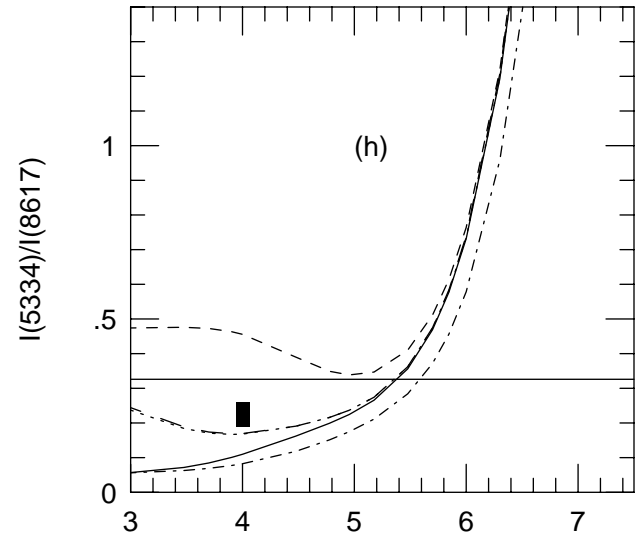
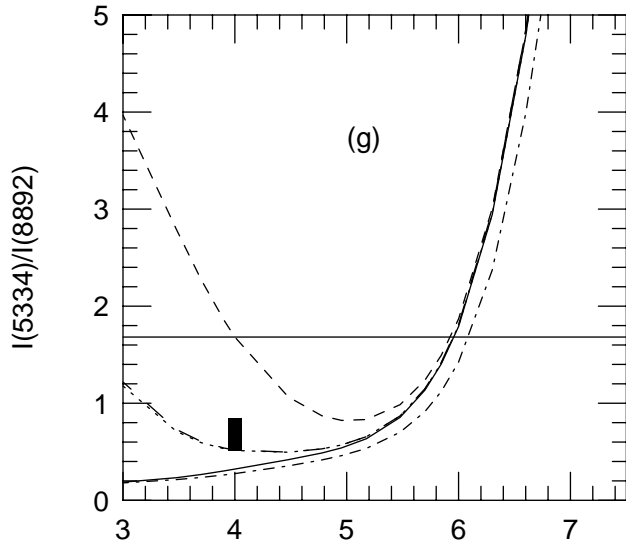


$\log_{10}(T)$ (K)

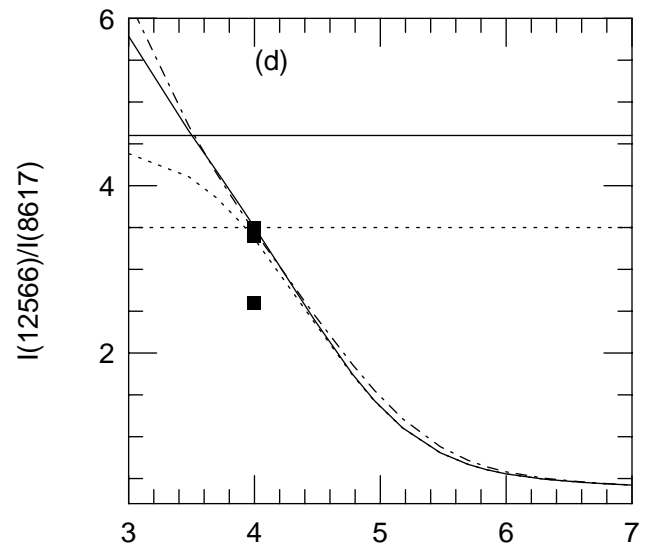
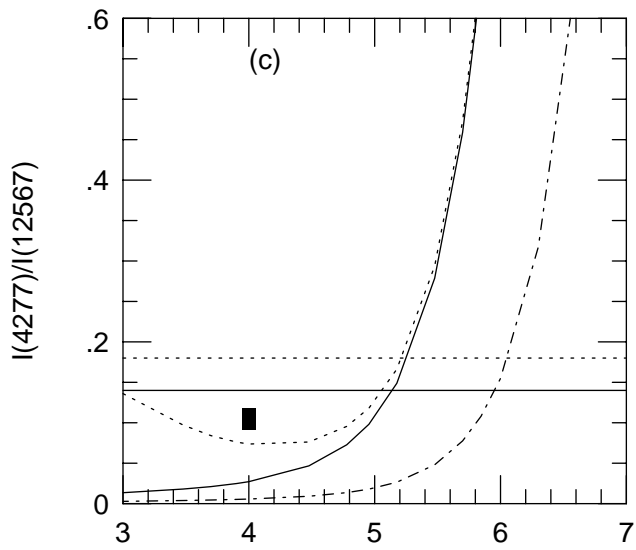
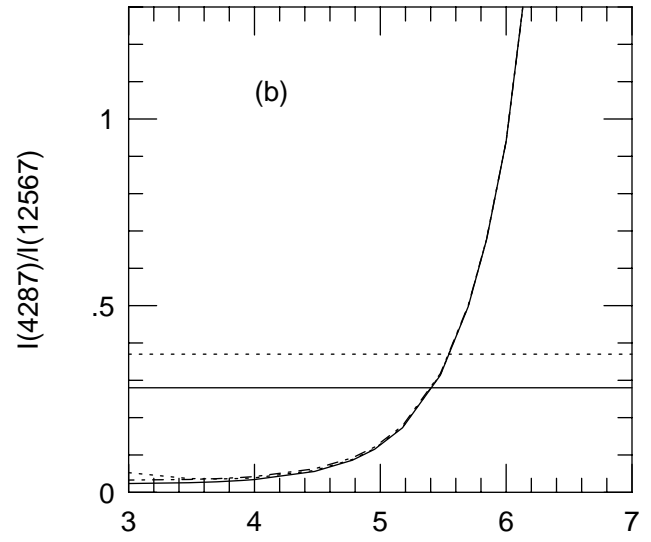
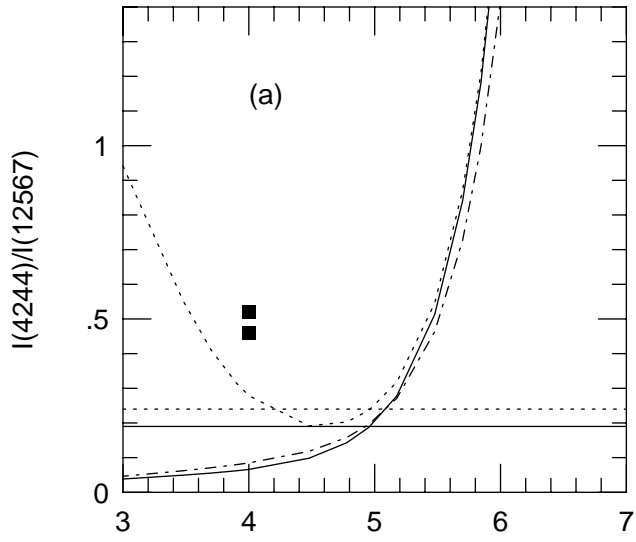




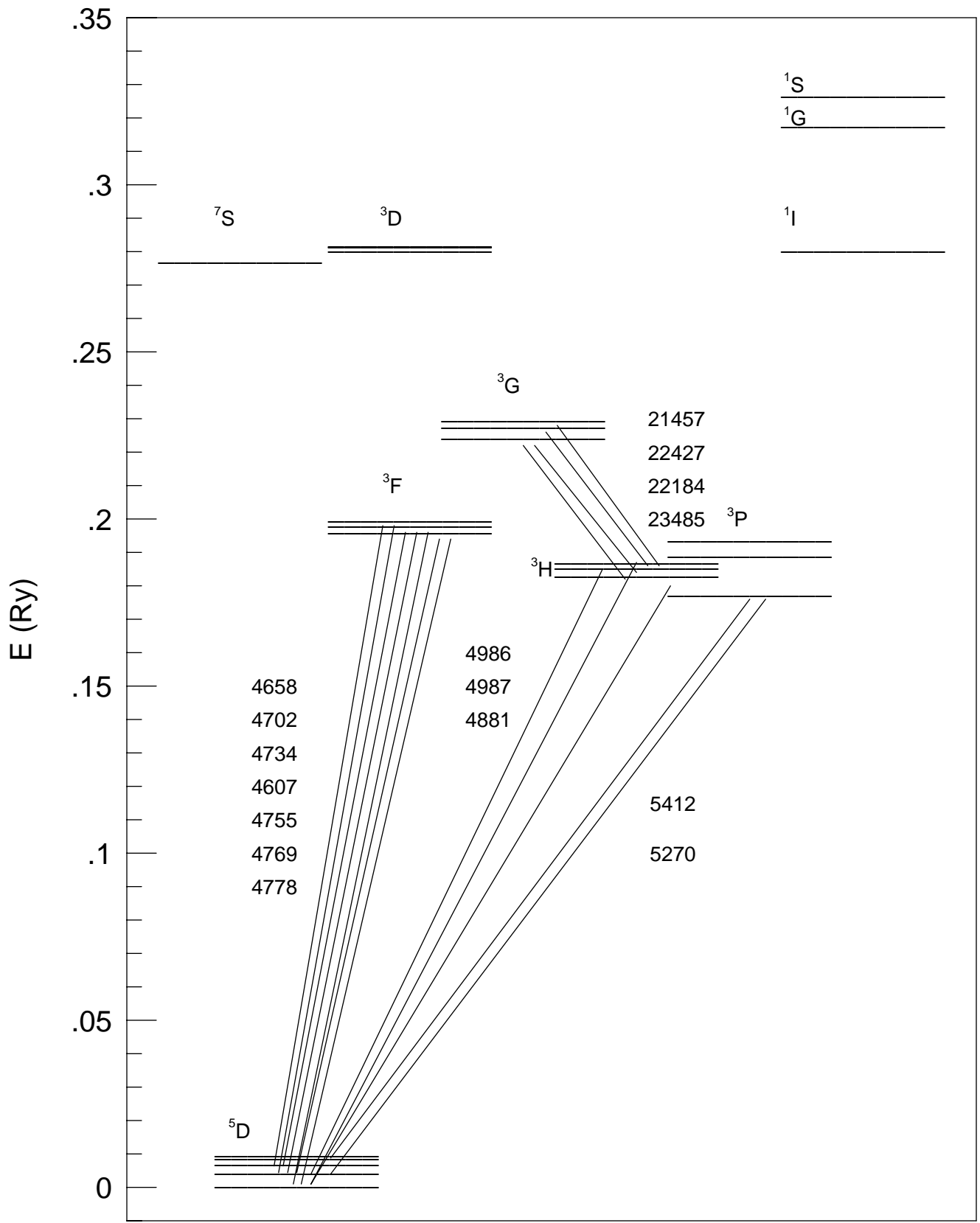
log N_e

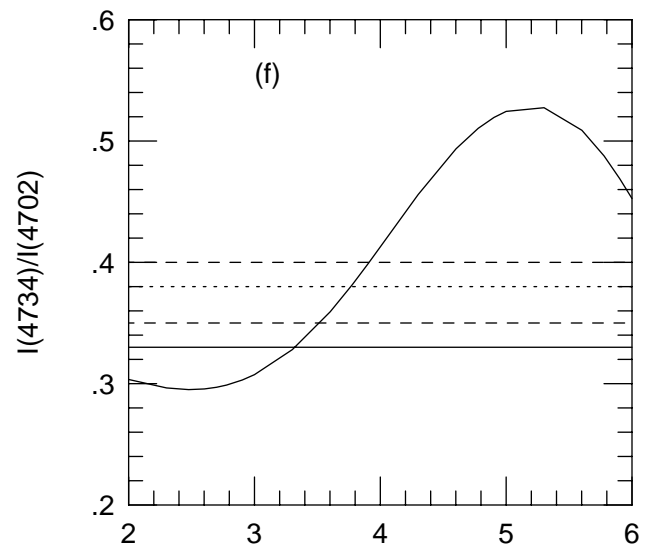
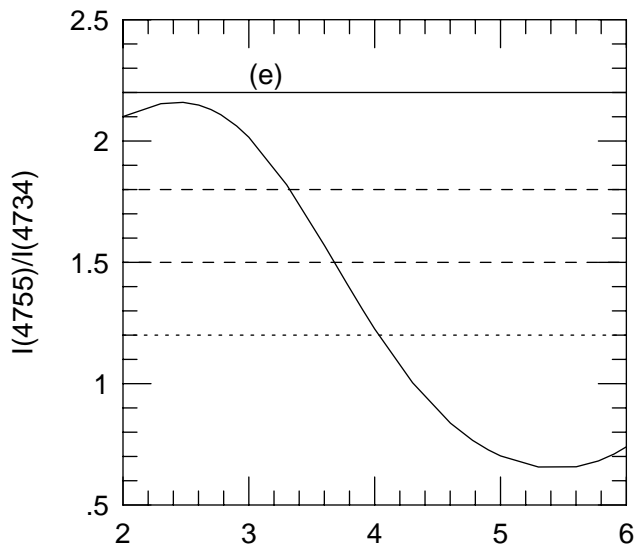
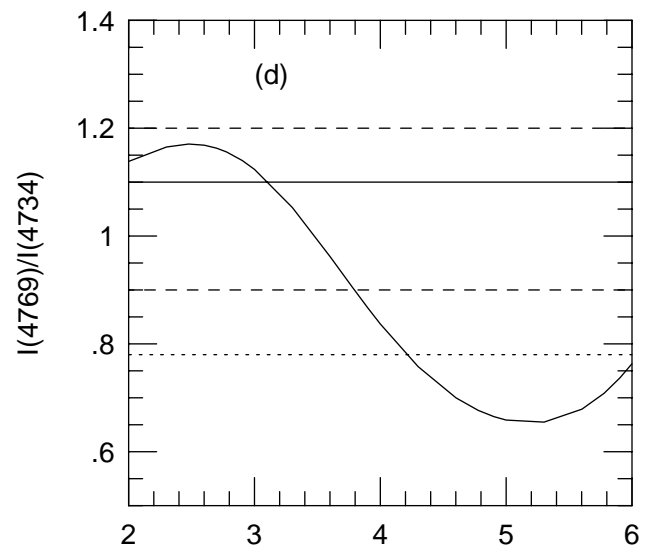
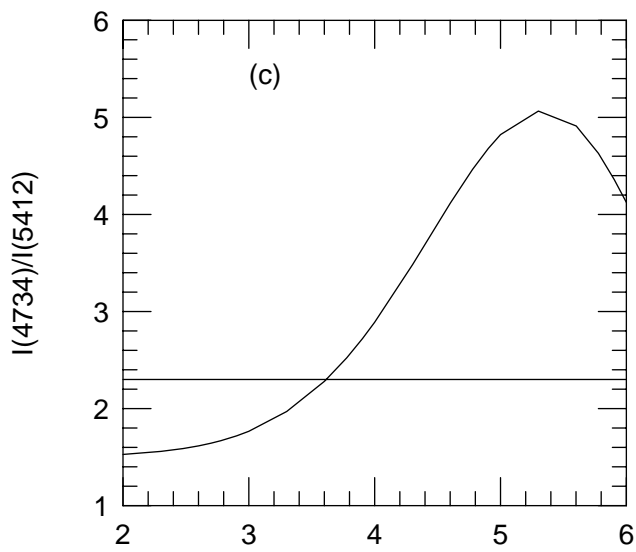
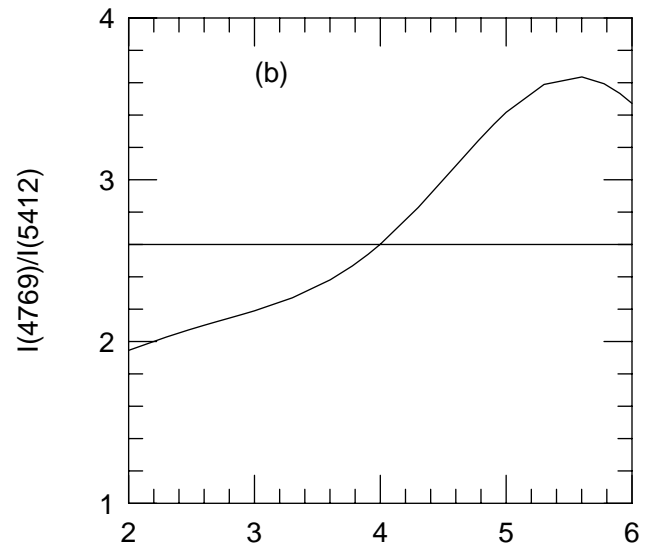
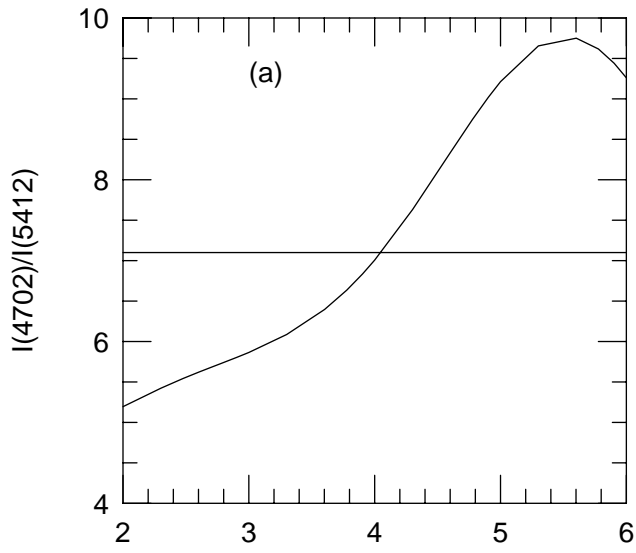


$\log N_e$

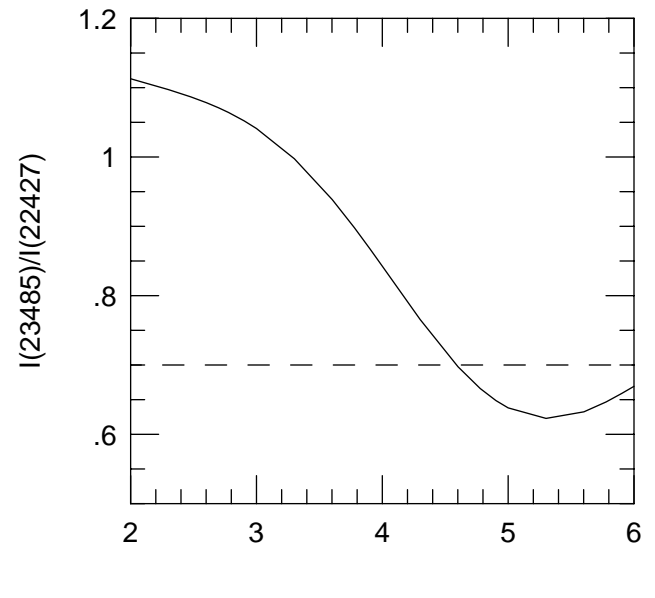
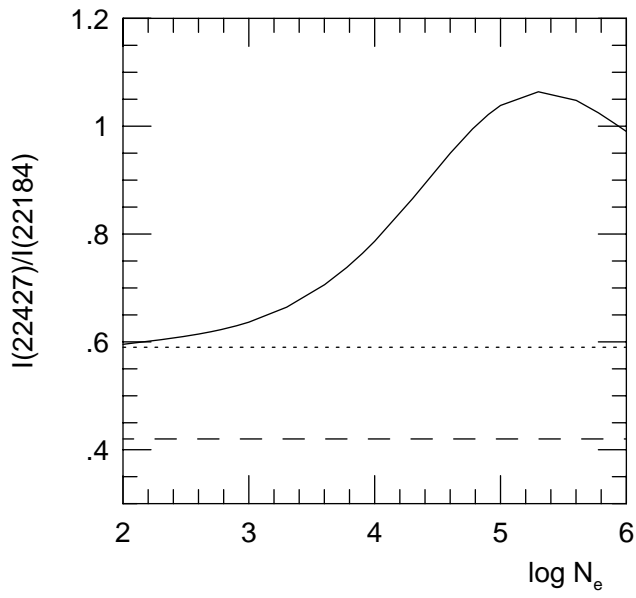
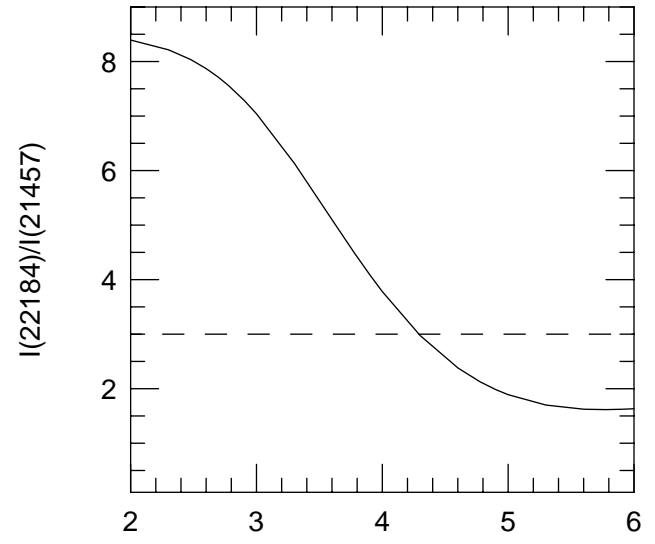
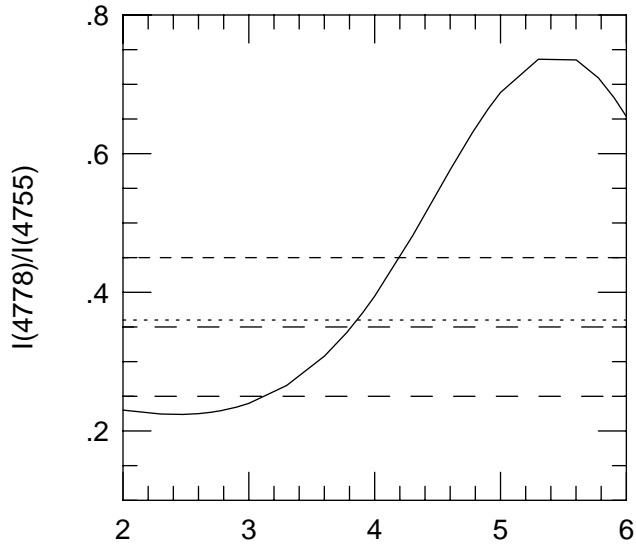


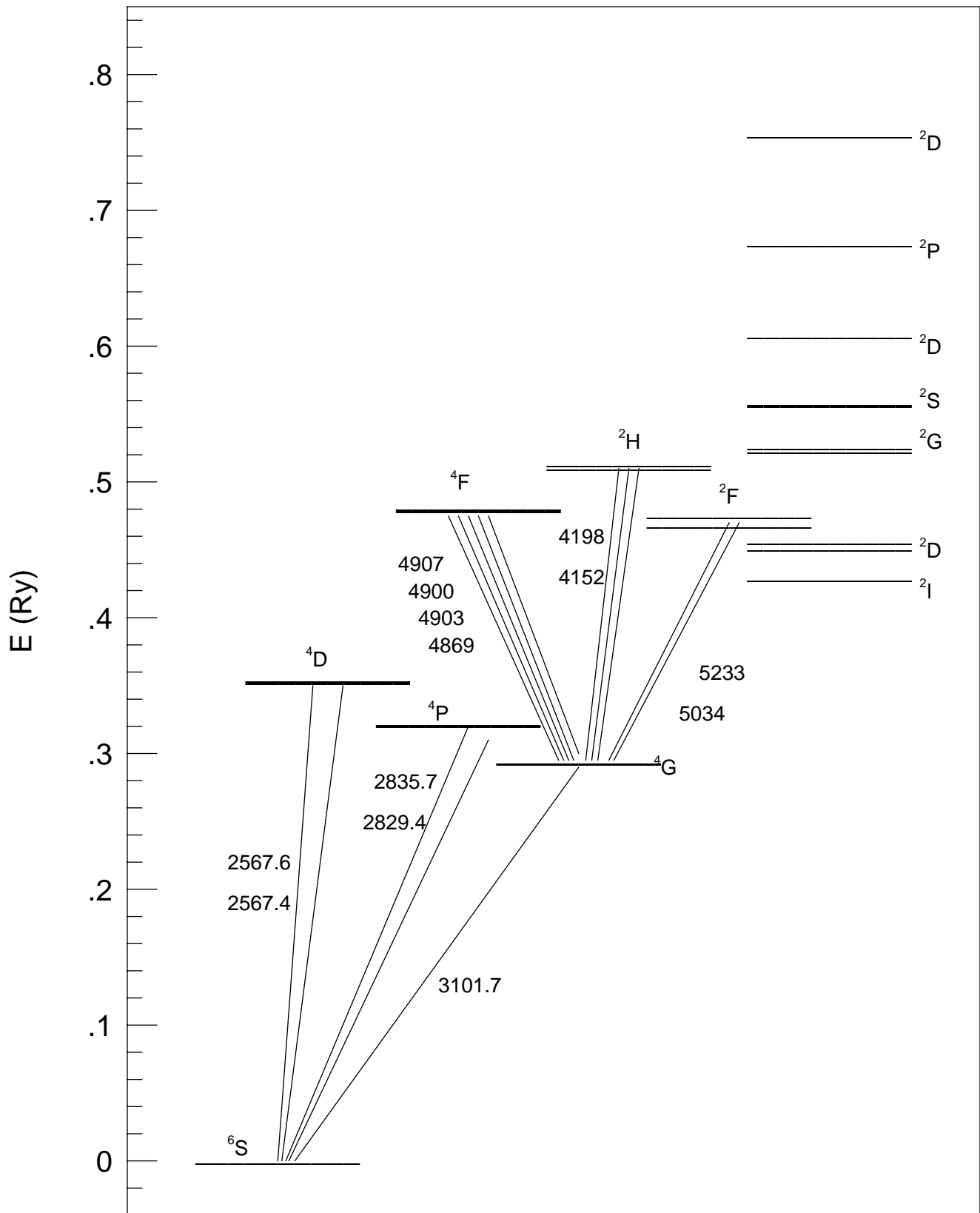
$\log N_e$

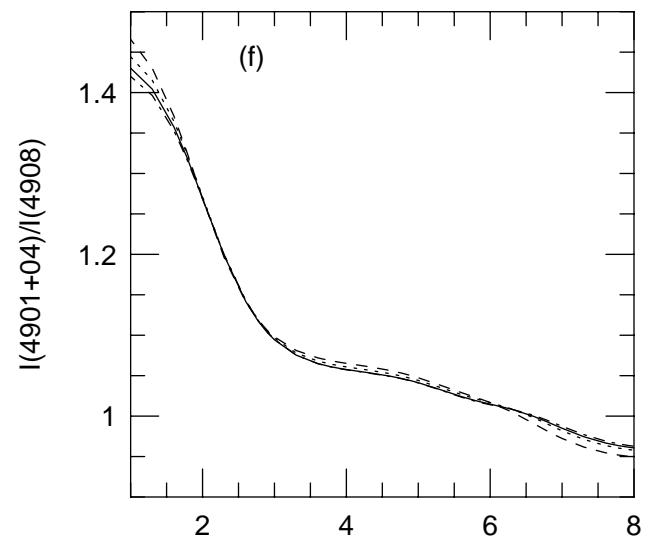
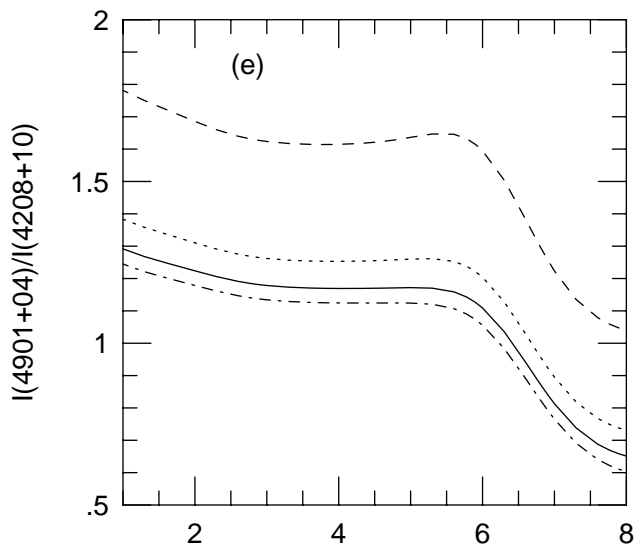
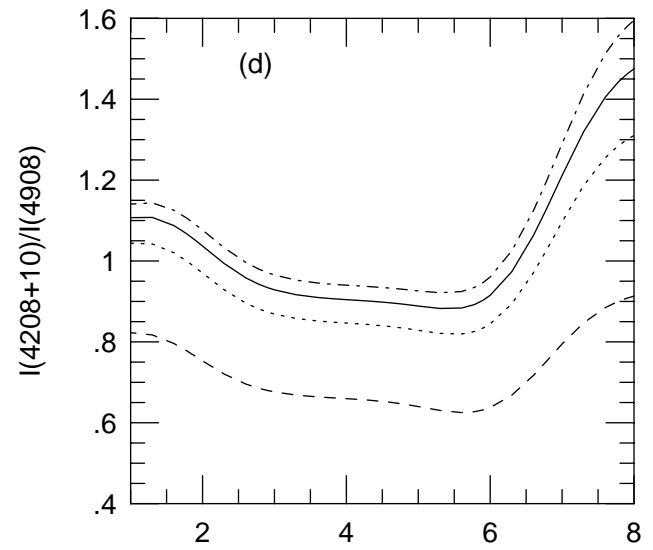
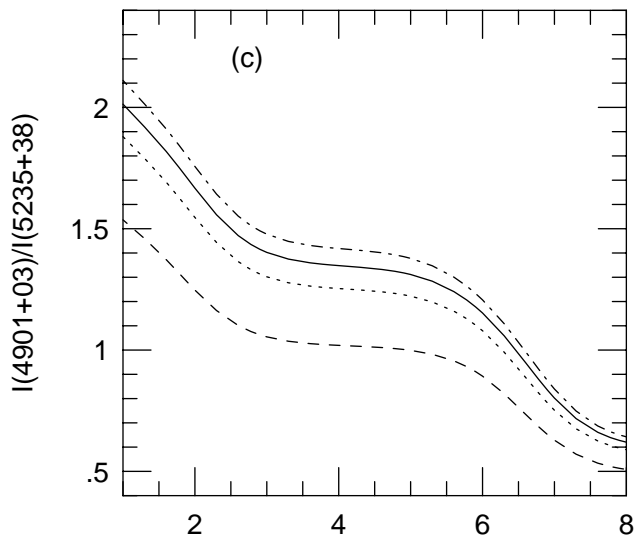
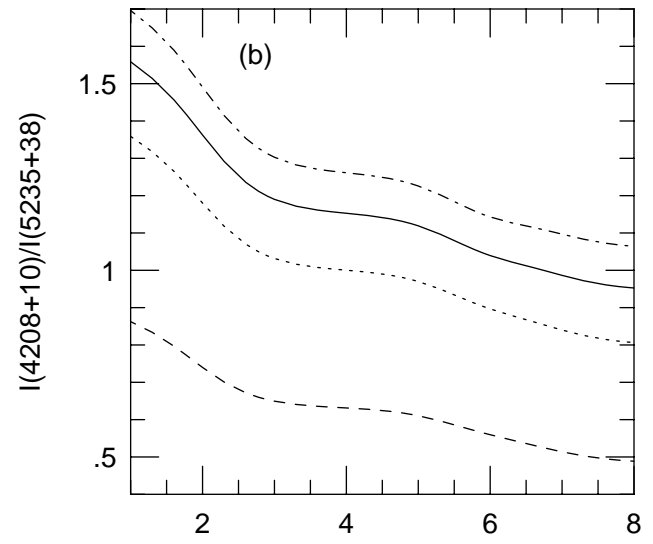
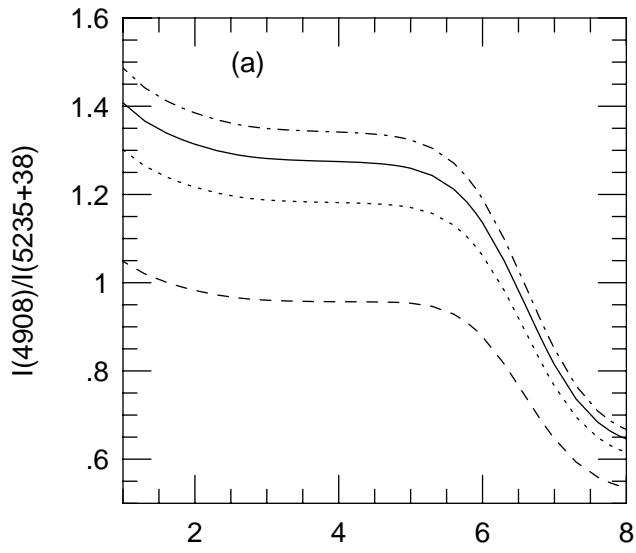




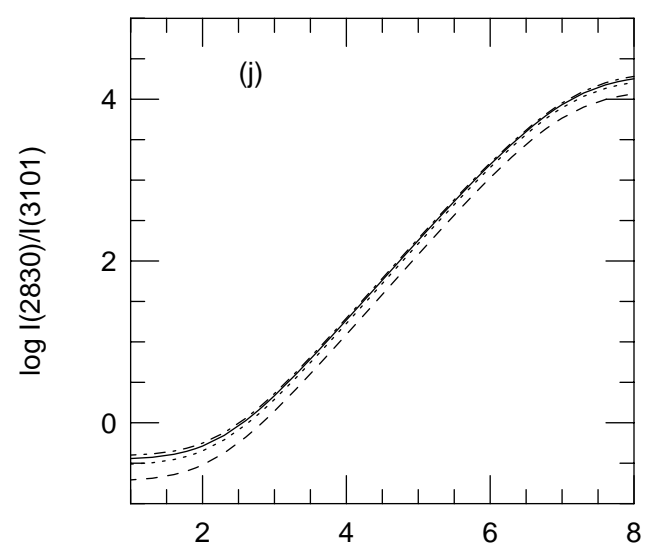
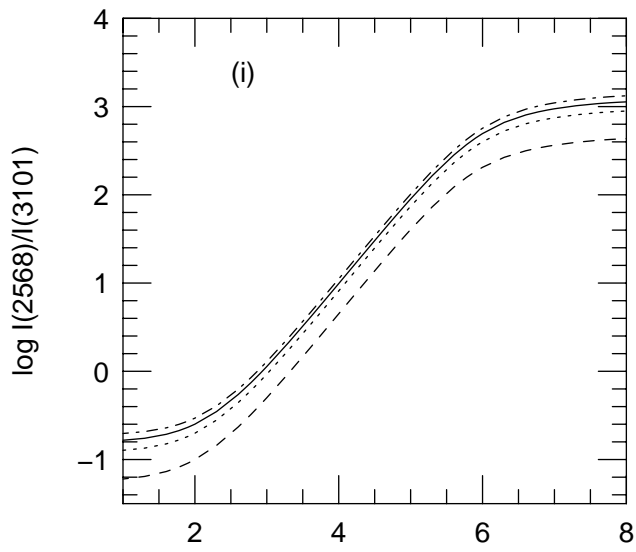
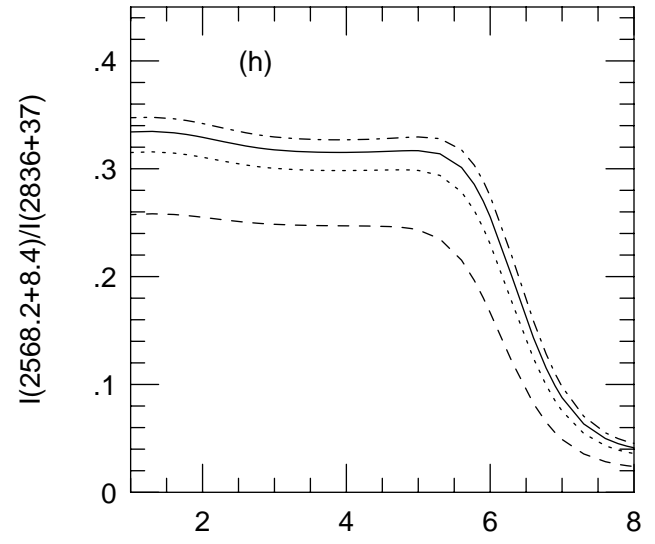
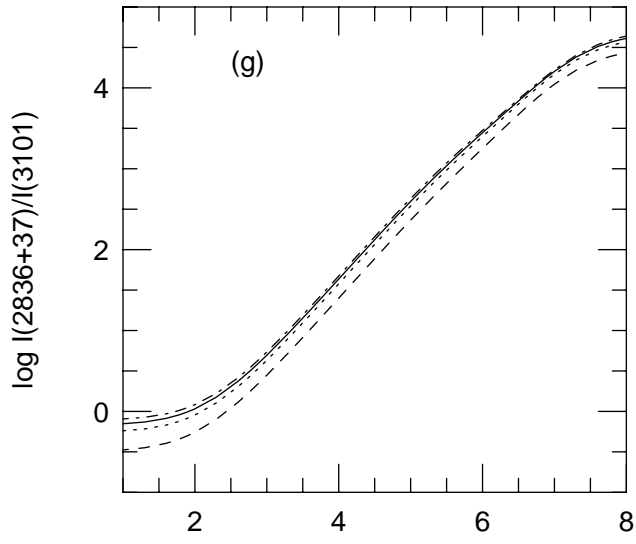
log N_e







log N_e



$\log N_e$

